THE EFFECT OF ASPERITY GEOMETRY ON ELASTIC-PLASTIC STATISTICAL AND MULTI-SCALE ROUGH SURFACE CONTACT MODELS

by

Nolan Ryan Chu

A thesis submitted to the Graduate Faculty of
Auburn University
in partial fulfillment of the
requirements for the Degree of
Master of Science

Auburn, Alabama
May 5, 2018

Keywords: Spherical Asperity, Greenwood-Williamson Model, Rough Surface Contact, Multi-scale Model, Elastic-Plastic, Sinusoidal Asperity

Copyright 2018 by Nolan Ryan Chu

Approved by

Robert L. Jackson, Chair, Professor of Mechanical Engineering
Dan Marghitu, Professor of Mechanical Engineering
Hareesh Tippur, McWane Endowed Chair Professor of Mechanical Engineering

ABSTRACT

The solution to an elastic-plastic contact problem can be applied to many phenomena such as friction, wear, and thermal contact resistance. Many models have been developed to solve it. A deterministic approach accurately describes the entire surface, but its computational time is too long for practical use. Thus, simplified mathematical models have been developed to describe rough surface contact. Older models employed a statistical methodology to solve the contact problem, and they borrowed the solution for spherical contact to represent individual asperities. However, it is believed that a sinusoidal geometry may be more realistic. This geometry has also been applied to a newer mathematical model: the multiscale model. All models predict similar qualitative trends, but their quantitative results diverge. This work highlights the disparities between them when applied to a piston ring-cylinder wall interface as well as two reference surfaces in contact with a rigid flat. For the reference surfaces, they were compared to a deterministic FEM model.

ACKNOWLEDGEMENTS

I would like to thank Ford Motor Company for funding this project as a part of the Ford University Research Program.

TABLE OF CONTENTS

LIST OF TABLES

LIST OF FIGURES

LIST OF SYMBOLS

ω	interference between surfaces
z	surface height
d	separation of mean asperity height
$\overline{A}$	contact area of individual asperity
R	asperity radius
$\overline{P}$	contact force of individual asperity
P	total contact force
E	elastic modulus
v	Poisson's ratio
η	asperity density per unit area
A_n	nominal contact area
A_r	real contact area
N	total number of asperities
N_c	number of asperities in contact
ϕ	distribution function for asperity heights (assumed to be Gaussian throughout this work)
σ	standard deviation of surface heights
m_2	second spectral moment
m_4	fourth spectral moment
σ_s	standard deviation of asperity heights

α	bandwidth parameter
ω_c	critical interference between surfaces
S_y	yield strength
f	surface frequency
Δ	surface amplitude
p^*	pressure required for complete elastic contact
A_p	elastic-plastic contact area for single sinusoidal asperity
p^*_{ep}	pressure required for complete elastic-plastic contact
Δ_c	critical amplitude for elastic-plastic contact
G	nondimensionalized gap between surfaces
g	gap between surfaces
A_i	total contact area on i^{th} scale

CHAPTER 1

INTRODUCTION

Contact between rough surfaces is a ubiquitous problem that can be applied to numerous phenomena such as friction, wear, and contact resistance. It can be modeled in many ways such as statistical [1-4], fractal [5], and multi-scale [6] models. In the statistical model, the surface is generalized by using mathematical parameters to calculate probabilities to determine the contact area and force. Fractal based models account for different scales of surface features neglected by statistical models. Due to their limitations such as predicting zero contact area, they are not considered in this work. The multi-scale model more accurately incorporates deformation mechanics and is not restrained to zero area of contact at the smallest scales, which occurs if perfect fractal surfaces are assumed.

In this project, a combined contact mechanics and lubrication model was developed to predict performance in mechanical systems such as a piston ring system in a combustion engine. To represent the contact mechanics module, three different rough surface contact models were applied to it. The first two models were based on the Greenwood-Williamson (GW) statistical model, which assumes a Gaussian distribution of asperities. One model assumed the asperities were spherical in nature, while the other assumed sinusoidal asperities. Both assumed identical radius of curvature for each peak and a lack of interaction between adjacent asperities. However, the sinusoidal asperity model includes a periodic boundary condition which includes interactions with adjacent

asperities. The final model was the full multi-scale model with asperities assumed to be sinusoidal in shape and no underlying statistical distribution required because the surface would be analyzed in the frequency domain. The contact models are part of the flow chart seen in Figure 1.1 as displacements are iteratively calculated.

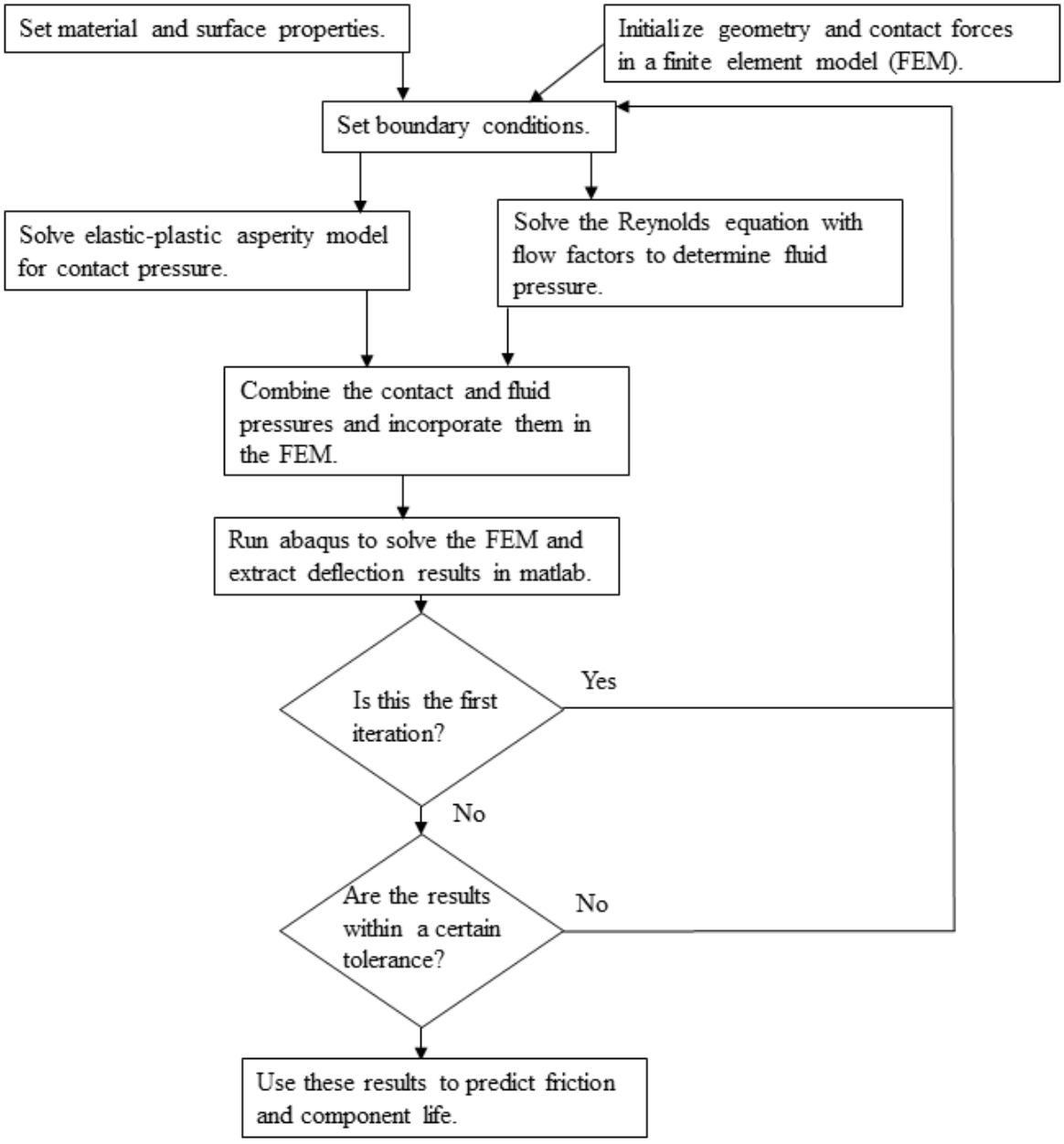

Figure 1.1: Flow chart of iterative calculations for the piston ring

CHAPTER 2

HISTORICAL BACKGROUND

2.1 Methods of Modeling Rough Surfaces

This chapter details various methods to model rough surface contact. Statistical, fractal, and multi-scale models are mentioned here, but surfaces can be modeled using other methods. They have unique assumptions and mathematical techniques, but they predict similar qualitative trends.

2.2 Statistical Methods

Henrich Hertz was one of the first researchers in the field of contact mechanics. He solved the elastic deformation of a parabola, which can be applied to cylindrical or spherical contact [7]. However, he did not consider the effects of friction or plastic deformation. His solution has been expanded from a single asperity, or raised point on a surface, to a system of asperities that describes a surface's topography.

One such expansion is the statistical model provided by Greenwood and Williamson [1], which shall be referred to as the GW model. Their work considered the interaction between two planes. One plane was perfectly flat and rigid, while the other was covered with identical spherical asperities. They assumed that asperities behave independently of each other and deformation was restricted to the asperities. The asperity heights were assumed to fit a Gaussian distribution, so the percentage of contact area

could be calculated using statistical mathematics. This model relies on the interference, or the material that deforms to maintain a given separation, between the surfaces.

The GW model only considers elastic contact, so the model has been refined to include the effects of elastic-plastic deformation. One such model was derived by Jackson and Green [3] (JG), which establishes the required load above which the statistical model predicts plastic deformation. Other models such as those proposed by Chang, Etsion, and Bogy (CEB) [2] and Kogut and Etsion [4] include the effects of plasticity, but they are not considered here because they contain discontinuities in crucial parameters. As the contact pressure increases, so does the internal stress within asperities, which causes yielding and plastic deformation. At the critical interference, which is provided in the next chapter, the material is assumed to yield, and JG model is used instead of Hertzian contact. The JG model is limited to small deformations such that the contact radius is 41% or less of the radius of curvature.

2.3 Fractal Methods

Statistical models are reliable and easily implemented, but shortcomings exist. For one, the entire surface is characterized by a single radius of curvature. Thus, they neglect the effects of different scales of features. Furthermore, the surface heights may be too far removed from a Gaussian distribution to employ the GW model. In this instance, other models must be used instead. Majumdar and Bhushan [5] (MB) created a fractal model for rough surface contact. They applied the Weierstrauss-Mandelbrot (WM) function to multiple levels of roughness. While it depicts a different roughness for each scale, a surface may not have a spectrum that can be related to the fractal equation.

Ciavarella et al. [8] solved a 2D W-M fractal-rigid flat interface using a stacked asperity assumption and an elastic sinusoidal model derived by Westergaard [9]. They found that the contact area approached zero as higher scales were included. For this reason, this work does not consider a fractal based model.

2.4 Multi-scale Methods

To overcome the limitations of the GW model and predict a realistic area of contact, the multi-scale model as developed by Jackson and Streator (JS) is used. Their model builds off Archard's [10] "protuberance upon protuberance" concept in which the Hertzian sphere was expanded by including hemispheres of smaller radii on it. As loads increase, the surfaces come into complete contact at the smallest scales and begin compressing at larger scales. Archard's experiments showed a linear relationship between area and force and that rougher surfaces would only flatten with larger force. Jackson and Streator refined Archard's model so it could be applied to real surfaces [6]. They made the following assumptions: smaller asperities are stacked on larger asperities, load is distributed equally over all asperities on each scale, total load does not depend on scale, and the contact area is limited to that of the scale below. They applied the Johnson, Greenwood, and Higginson piecewise solution [10] for perfectly elastic 3D sinusoidal contact and connected the equations. To consider roughness, the surface was converted using a discrete Fourier transform into a series of sine waves of known frequency and amplitude [6]. Their procedures will be discussed in more detail in the next chapter.

The JS model was subsequently modified using results from Krithivasan and Jackson [11], who analyzed a finite element model of a sinusoidal asperity. Like the JG model, a critical value below which contact remains perfectly elastic exists. Because

interference is not calculated, the critical values are found in terms of force. More details on their process are mentioned in the next chapter. The multi-scale model was extended by Gao and Bower [12], who included plastic deformation, albeit for a 2D model. Therefore, there work is not considered here.

CHAPTER 3

METHODS OF ANALYSIS

3.1 Introduction

In this chapter, the models being used to analyze rough surface contact are presented. Numerical techniques for calculating the real area of contact, the contact pressure, and the surface separation for elastic and elastic-plastic contact are given. Also, the critical values at which elastic-plastic contact starts are given.

3.2 Development of the GW Statistical Model

For each asperity in the GW model, the difference between its height and the average asperity height is z. When a rough surface is placed in contact with another surface, some asperities are compressed by a distance ω, which is defined as

$$\omega = z - d, \tag{3.1}$$

where d is the distance between the mean asperity heights for the surfaces put together. In the original GW model, the contact area and the force were adopted from the Hertz elastic contact model [7]. The equations for them are

$$\overline{A} = \pi R \omega \tag{3.2}$$

$$\overline{P} = \frac{4}{3} E' \sqrt{R} \omega^{\frac{3}{2}} \tag{3.3}$$

where E' is a modified elastic modulus calculated given the elastic moduli and Poisson's ratios of surfaces 1 and 2:

$$\frac{1}{E'} = \frac{1-\nu_1^2}{E_1} + \frac{1-\nu_2^2}{E_2} \tag{3.4}$$

The asperity radius R is a modified quantity as well, given by

$$\frac{1}{R} = \frac{1}{R_1} + \frac{1}{R_2}, \tag{3.5}$$

where R_1 and R_2 are the average asperity radii of surfaces 1 and 2 respectively.

To derive the total contact area and pressure under the GW model [1], the asperity density per unit area, η, and the nominal contact area, A_n, must be known. The product of these quantities will be called the asperity count, N. The asperities in contact, N_c, can be found using the integral

$$N_c = A_n \eta \int_d^\infty \phi(z)\, dz, \tag{3.6}$$

where ϕ represents the probability density function for the normal distribution with a zero mean and standard deviation, σ.

Thus, the total contact area and force can be found as follows:

$$A(d) = A_n \eta \int_d^\infty \overline{A}(z-d)\,\phi(z)\, dz, \tag{3.7}$$

$$P(d) = A_n \eta \int_d^\infty \overline{P}(z-d)\,\phi(z)\, dz. \tag{3.8}$$

These integrals were evaluated numerically using Simpson's Rule. The asperity density, asperity radius, and root mean square of the asperity heights were calculated using a spectral moment approach derived by McCool [13]. The spectral moments were found from raw surface data using the following equations:

$$m_2 = \frac{1}{N}\sum_{n=1}^{N}\left(\frac{dz}{dx}\right)_n^2, \tag{3.9}$$

$$m_4 = \frac{1}{N}\sum_{n=1}^{N}\left(\frac{d^2z}{dx^2}\right)_n^2. \tag{3.10}$$

where N is the number of points where the surface height was measured. For a three-dimensional surface, the moments were calculated along two orthogonal directions, then averaged together. They were then used to calculate the statistical quantities as follows:

$$\eta = \frac{m_4}{6\pi\sqrt{3}m_2} \tag{3.11}$$

$$R = 0.375\sqrt{\frac{\pi}{m_4}} \tag{3.12}$$

$$\sigma_s = \sqrt{\sigma^2 - \frac{0.0003717}{\eta^2 R^2}} \tag{3.13}$$

To check if the surface was Gaussian in nature, the bandwidth parameter α was calculated in both dimensions using the equation

$$\alpha = m_4\left(\frac{\sigma}{m_2}\right)^2. \tag{3.14}$$

If the value of α exceeded 1.5, then the surface was assumed to be sufficiently Gaussian in that direction, and the G-W model could be used confidently.

However, elastic contact is not realistic because asperities yield when the applied pressure reaches a critical value, especially for metallic surfaces. At the initial point of yielding, the surface compression is ω_c. Jackson and Green [3] derived this analytical solution using the von Mises criterion:

$$\omega_c = R\left(\frac{\pi C S_y}{2E'}\right)^2, \tag{3.15}$$

where S_y is the yield strength of the material and

$$C = 1.295e^{0.736\nu}. \tag{3.16}$$

At interference values below $\omega/\omega_c \leq 1.9$, the elastic contact formulae were still approximately valid. At higher values of deflection, the following equations were used to predict contact area and force:

$$\overline{A} = \pi R\omega\left(\frac{\omega}{1.9\omega_c}\right)^B \tag{3.17}$$

$$\overline{P} = \overline{P_c}\left\{\left[e^{-0.25\left(\frac{\omega}{\omega_c}\right)^{\frac{5}{12}}}\right]\left(\frac{\omega}{\omega_c}\right)^{\frac{3}{2}} + \frac{4H_G}{CS_y}\left[1 - e^{-0.04\left(\frac{\omega}{\omega_c}\right)^{\frac{5}{9}}}\right]\frac{\omega}{\omega_c}\right\}, \tag{3.18}$$

where

$$B = 0.14e^{23e_y}, \tag{3.19}$$

$$e_y = \frac{S_y}{E'}, \tag{3.20}$$

$$\frac{H_G}{S_y} = 2.84\left[1 - e^{-0.82\left(\sqrt{\frac{\omega}{R}}\left(\frac{\omega}{1.9\omega_c}\right)^{\frac{B}{2}}\right)^{-0.7}}\right], \tag{3.21}$$

$$\overline{P_c} = \frac{4}{3}\left(\frac{R}{E'}\right)^2\left(\frac{C\pi S_y}{2}\right)^3 \tag{3.22}$$

3.3 Application of Sinusoidal Asperities to the GW Model

Alternatively, the asperities could be assumed to have a sinusoidal profile and evenly distributed based on η. At their peaks, their radius of curvature was identical and

defined by R. The following relations were used to convert the asperity radius and density to the parameters for sinusoidal asperities, frequency and amplitude [14]:

$$f = \sqrt{\frac{\eta}{2}}, \tag{3.23}$$

$$\Delta = \frac{1}{4R\left(f\pi\right)^2}. \tag{3.24}$$

Johnson, Greenwood, and Higginson (JGH) [9] developed a piecewise defined function between pressure and contact area for a single asperity under elastic loading. In their equations, $\bar{p}$ is the average contact pressure, and p^* is the pressure required for complete contact, which is given by

$$p^* = \sqrt{2}\pi E' f \Delta. \tag{3.25}$$

The ratio of the contact pressure and the pressure required for complete contact shall be called P_e. At pressures below p^*, JGH were not able to derive a closed form solution, but rather provided two asymptotic solutions based on Hertz contact. For P_e<< 1,

$$\left(\overline{A}_{JGH}\right)_1 = \pi\lambda^2\left[\frac{3P_e}{8\pi}\right]^{\frac{2}{3}}, \tag{3.26}$$

while at large values of P_e,

$$\left(\overline{A}_{JGH}\right)_2 = \frac{\lambda^2}{2}\left(1 - \frac{3}{2\pi}\left[1 - P_e\right]\right). \tag{3.27}$$

Jackson and Streator [6] fitted a polynomial that combined the two equations above using experimental data from Johnson et. al:

For P_e<0.8,

$$\widetilde{A} = \left(\overline{A}_{JGH}\right)_1\left(1 - P_e^{0.51}\right) + \left(\overline{A}_{JGH}\right)_2 P_e^{1.04} \tag{3.28}$$

For $P_e \geq 0.8$,

$$\widetilde{A} = \left(\overline{A}_{JGH}\right)_2 \tag{3.29}$$

These equations neglect asperity yielding, so an elastic-plastic model for large loads was developed by Krithivasan and Jackson [11]. Their equation for the contact area at low pressures when plastic deformation occurs is

$$A_p = 2\left(\frac{A_c}{2}\right)^{\frac{1}{1+d}}\left(\frac{3\overline{p}}{4Cf^2 S_y}\right)^{\frac{d}{1+d}}, \tag{3.30}$$

where

$$d = 3.8\left(\frac{E' f\Delta}{S_y}\right)^{0.11}, \tag{3.31}$$

and

$$A_c = \frac{2}{\pi}\left(\frac{CS_y}{8E' f^2\Delta}\right)^2 \tag{3.32}$$

is the critical area at which elastic-plastic contact begins. They also found that complete contact occurs at much lower pressures compared to a purely elastic model and called that value $p^*_{ep.}$ The ratio of the contact pressure, $\overline{p}$, and p^*_{ep} is P_{ep}.

Their equation linking contact area and load over low pressures and high pressures is

$$\overline{A} = A_p\left(1 - P_{ep}^{1.51}\right) + \left(\overline{A}_{JGH}\right)_2 P_{ep}^{1.04}. \tag{3.33}$$

In this equation, the value of $\left(\overline{A}_{JGH}\right)_2$ is calculated by replacing P_e with P_{ep}. They also derived a critical average contact pressure below which contact remains in the elastic regime. Because that was derived from spherical contact, Jackson et. al. [15] derived a

new model by computing the critical interference Δ_c, above which elastic-plastic relations are used. Their corrected expression for it as published by Ghaednia et. al. [16] is

$$\Delta_c = \frac{\sqrt{2}S_y}{E' f \pi \left[3e^{-\frac{2}{3}(\nu+1)} + 2\left(\frac{1-2\nu}{1-\nu}\right)\right]}. \tag{3.34}$$

Using this value of critical interference, a new equation for p^*_{ep} that relates it to p^* was fitted to the FEM data of Krithivasan and Jackson [11],

$$\frac{P^*_{ep}}{p^*} = 0.992^{\left[\left\{\frac{\Delta}{\Delta_c}\right\}^{\frac{10}{3}\left(\frac{\Delta}{\Delta_c}\right)^{-0.39}+\frac{9}{4}\nu^4+0.64}-1\right]} \tag{3.35}$$

where

To apply sinusoidal asperities to the GW model, the surface separation must be known as well. Rostami and Jackson [17] derived expressions for elastic and elastic-plastic contact by extracting surface separation from a finite element model and averaging over the entire surface. Their fitted equations are

$$G = \left(1-\sqrt{P_e}\right)^{2.5} \tag{3.36}$$

for elastic contact and

$$G = \left(1-P_{ep}^{\,A_1 P_{ep}+A_2}\right)^{2.5} \tag{3.37}$$

for elastic-plastic contact. In these equations,

$$G = \frac{g}{\Delta}, \tag{3.38}$$

$$A_1 = -0.08\ln B^*, \tag{3.39}$$

$$A_2 = \frac{1}{15}\left(B^* - 1\right)^{0.44} + 0.99^{0.41\left\{B^* - 1\right\}} - 0.5, \tag{3.40}$$

$$B^* = \frac{\Delta}{\Delta_c} \tag{3.41}$$

3.4 Full Multiscale Model

The third model for rough surface contact considered in this work was iterative [6], as it incorporated the effects of asperities at different scales. The surface is first transformed to the frequency domain by performing a two-dimensional FFT. Its wavelength, λ, was set to be the length of the surface considered divided by the number of nodes. The applied force was a known quantity. Because the model requires a 1 to 1 correspondence between amplitudes and frequencies, the 1D Fourier coefficient was calculated using the equation

$$\beta_k = 0.5\left[\sqrt{\sum_{k_y=0}^{N_y-1}\left|z\left(k,k_y\right)\right|^2} + \sqrt{\sum_{k_x=0}^{N_x-1}\left|z\left(k_x,k\right)\right|^2}\right], \tag{3.42}$$

where z is the height of the surface [18]. In the analysis of [6], the number of asperities at each contact level was calculated. This model determines area over the entire level. The spectrum is symmetric, so only half the frequency levels are considered. For the lowest frequency, the area and force were defined as their nominal values. On each scale i, the overall contact area and force were calculated using the equations

$$A_i = \min\left(\frac{\widetilde{A}_i}{\lambda^2} A_{i-1}, A_{i-1}\right) \tag{3.43}$$

and

$$\overline{p_i} = \overline{p_{i-1}} \frac{F}{A_{i-1}}. \tag{3.44}$$

In Eq. 3.43, $\widetilde{A_i}$ is the area calculated using Equation 3.28 for elastic contact and Equation 3.33 for elastic-plastic contact. The total contact area and pressure were the values calculated after all the scales are included.

Unlike statistical models, the multiscale model does not require the gap between surfaces to be defined to calculate contact area as a function of force. For the lubrication model, that is a known quantity, so Equations 3.36-3.41 are used to calculate surface separation given the pressure.

CHAPTER 4

RESULTS

4.1 Cylinder Wall-Rigid Flat Interface

This study used measurements from two rough surfaces to compare contact models. The first surface analyzed was a cylinder wall from an internal combustion engine; it was placed in contact with a rigid flat. The rough surface of a 1 mm^2 area was measured using a DekTak 150 profilometer, and surface heights were reported at 1 μm intervals. Figure 1 shows the measured profile of the surface.

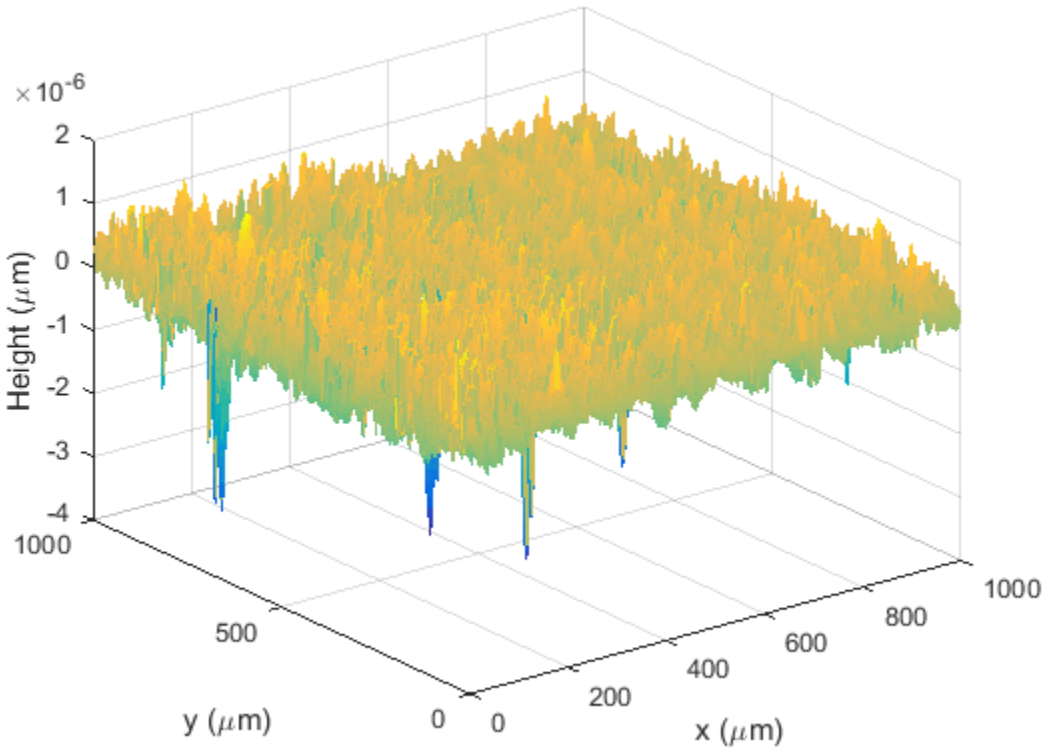

Figure 4.1: current production engine cylinder wall

The surface was leveled by performing a linear regression on each row of measurements, then zeroed by subtracting the average height from each point. Eq. 3.9-3.13 were applied to it, and the parameters extracted from the measured surface are summarized in Table 4.1.

Table 4.1: Cylinder Wall Parameters

	"x-direction"	"y-direction"	"averaged directions"
R (m)	$1.03*10^{-5}$	$1.39*10^{-4}$	$7.48*10^{-5}$
η ($1/m^2$)	$1.73*10^{10}$	$4.11*10^{8}$	$8.84*10^{9}$
σ_s (m)	$2.14*10^{-7}$	#	$2.38*10^{-7}$
α	4.338	0.4557	5.8417

This computation resulted in an imaginary number. This is because the surface heights in that direction are too heavily skewed from a Gaussian distribution.

The value of α_y was less than the threshold of 1.5, so that set of parameters was discarded. The two valid sets of statistical values were employed in the G-W model with spherical asperities, along with the material properties in Table 4.2.

Table 4.2: Material Properties of the Cylinder Wall

Property	Value
E	96.5 GPa
E'	51.7 GPa
v	0.26
S_y	220 MPa

To calculate the contact area and pressure, Eq. 3.7 & 3.8 were evaluated numerically using Simpson's method. The upper bound was set to be 10 σ_s, above which the effects of surface contact were assumed to be negligible. The average nominal pressure, or the force divided by the nominal area, was nondimensionalized by dividing by E'.

Because real asperities may resemble waves more than spheres, an alternative model that assumes sinusoidal asperities was employed as well. The statistical parameters were transformed into an amplitude and a frequency that described the surface. Table 4.3 summarizes these values for the cylinder wall.

Table 4.3: Sine Wave Parameters for Cylinder Wall

Parameter	"x-direction"	"averaged directions"
Δ (m)	$2.85*10^{-7}$	$7.66*10^{-8}$
λ (m)	$1.08*10^{-5}$	$1.50*10^{-5}$

The limits of integration remained constant; Equations 3.37-3.42 for contact pressures using bisection, which were combined with the amplitude and frequency to create a function for contact area. The integrals were evaluated with the same incremental length and method.

The surface was also analyzed by considering different roughness scales for use in the multiscale model. Figure 4.2 is a plot of the surface in the frequency domain. For the multiscale model, the force was varied between $5*10^{-21}$ and 500 N.

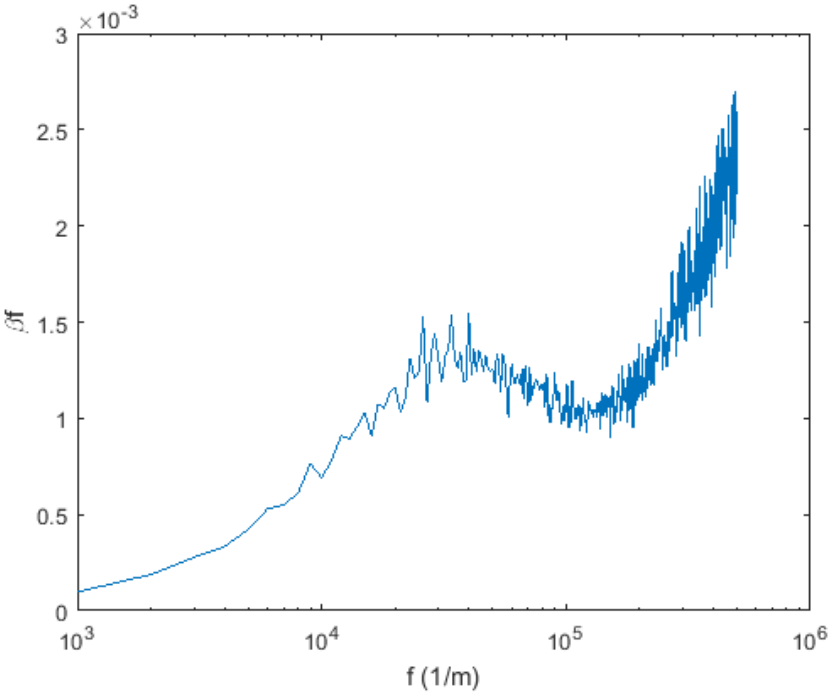

Figure 4.2: Spectrum of current production engine cylinder wall

In the following plots, contact areas or loads below 10^{-10} were assumed to be negligible and are not shown. Figures 4.3-4.5 plot the analysis using the G-W model with spherical asperities and both sets of statistical parameters.

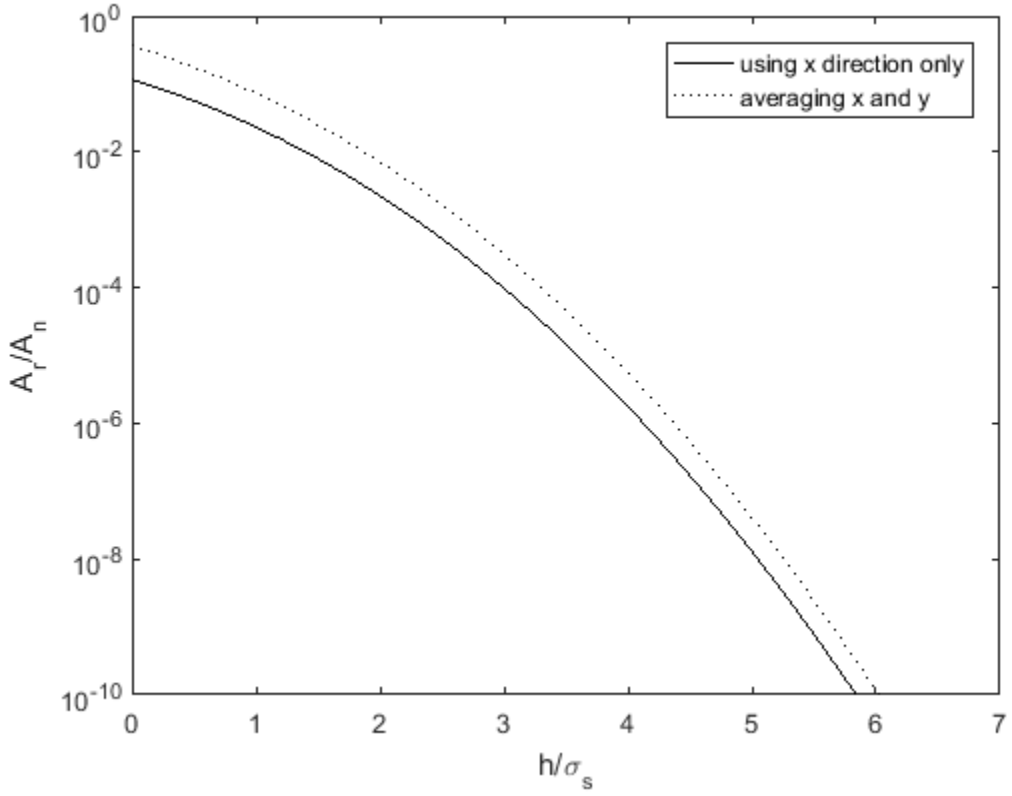

Figure 4.3: Area contact ratio for different surface separations, cylinder wall-rigid flat interface

Figure 4.3 shows a trend of decreasing area of contact as the surfaces become farther apart. Even at zero surface separation, there are substantial gaps between the surfaces. In other words, the contact area differs from the nominal contact area. Using just the spectral moments in the x direction to generate surface parameters underestimates the contact area.

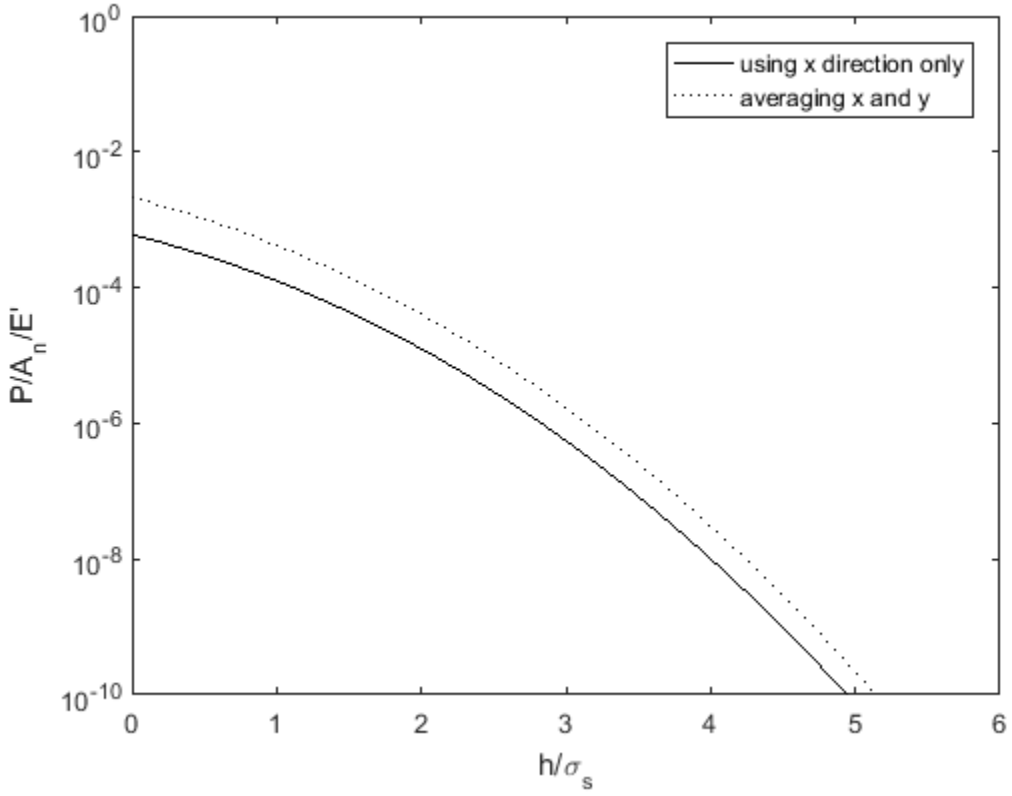

Figure 4.4: Pressure variation with surface separation, cylinder wall-rigid flat interface

Figure 4.4 displays a trend of decreasing contact pressure as surface separation increases, which makes sense. If only the spectral moments in the x direction are used to calculate statistical parameters, the contact pressure is underestimated in comparison to using moments in both directions. Also, the contact pressure decreases by several orders of magnitude, while surface separation increases by less than one order of magnitude.

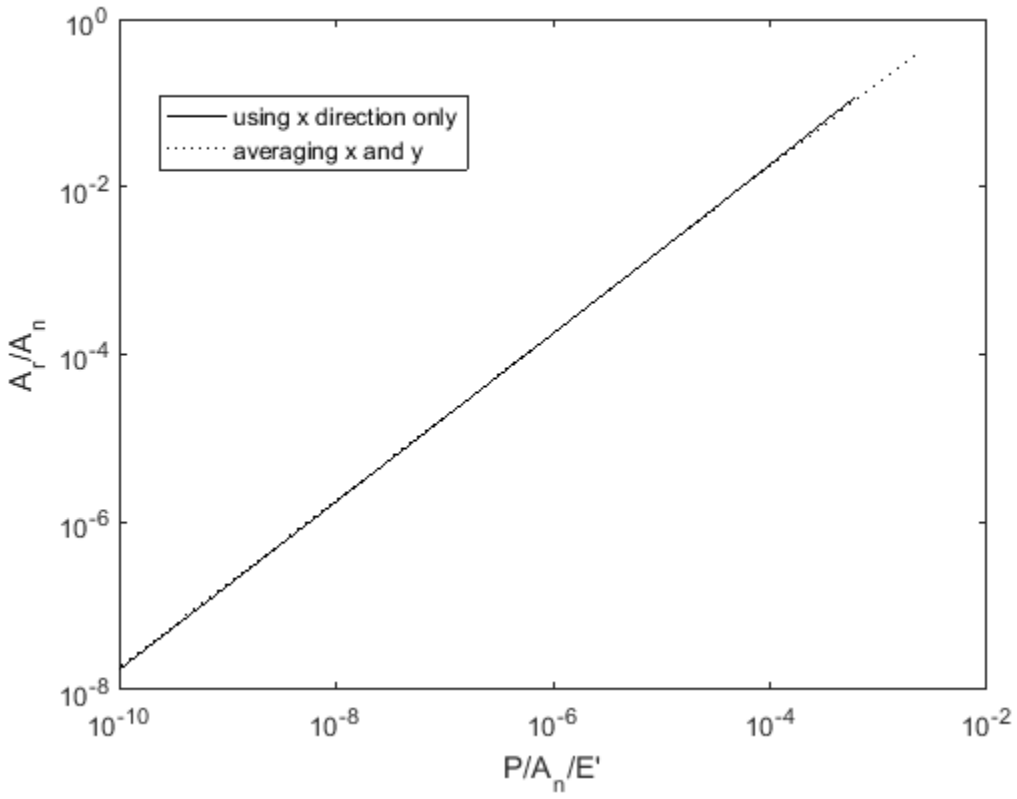

Figure 4.5: Area contact ratio and load comparison, cylinder wall-rigid flat interface

Figure 4.5 illustrates a nearly linear relationship between applied force and contact area, which is predicted by most rough surface contact models. While the surface's anisotropy affects the area and contact force relative to the surface separation, it does not affect the linear relationship between contact area and force. In fact, directional effects can be largely ignored.

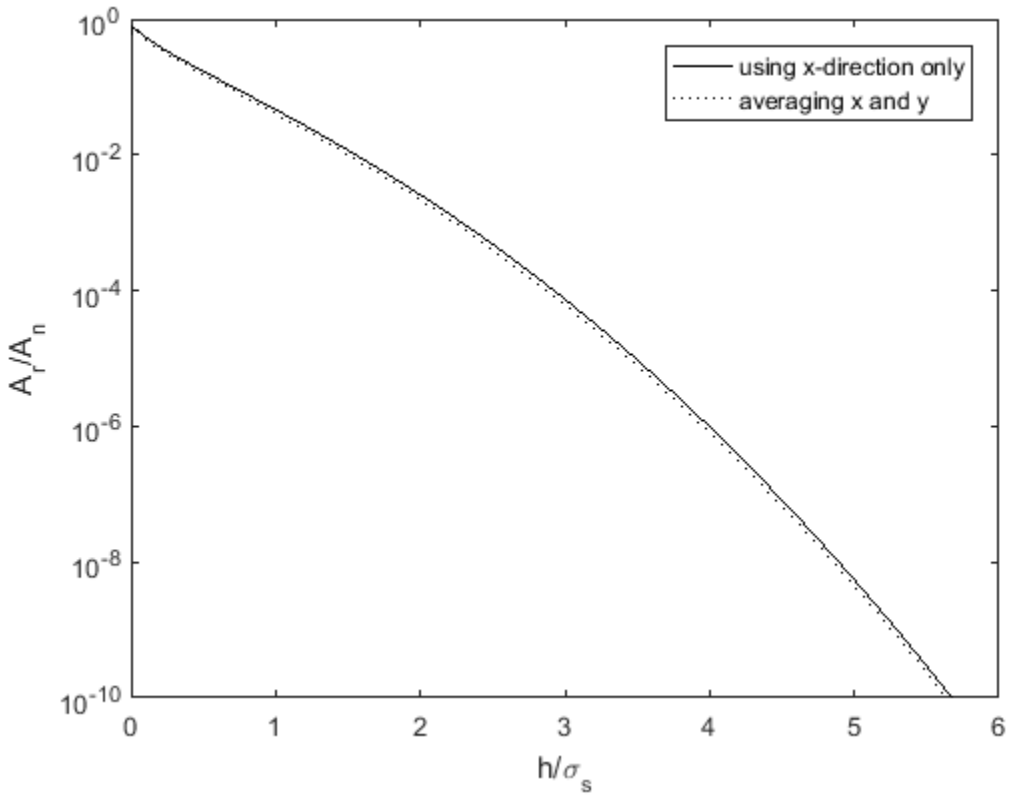

Figure 4.6: Area contact ratio over various surface separations for sinusoidal asperities, cylinder wall-rigid flat interface

Figure 4.6 shows results with sinusoidal asperities in the G-W model and compare them to the spherical asperity model. This plot does not show as large a difference in contact area ratio for the different sets of parameters compared to the model using spherical asperities. Also, this model predicts complete contact for zero surface separation. On the other hand, the spherical asperity model predicts that over half the surface will not be in contact.

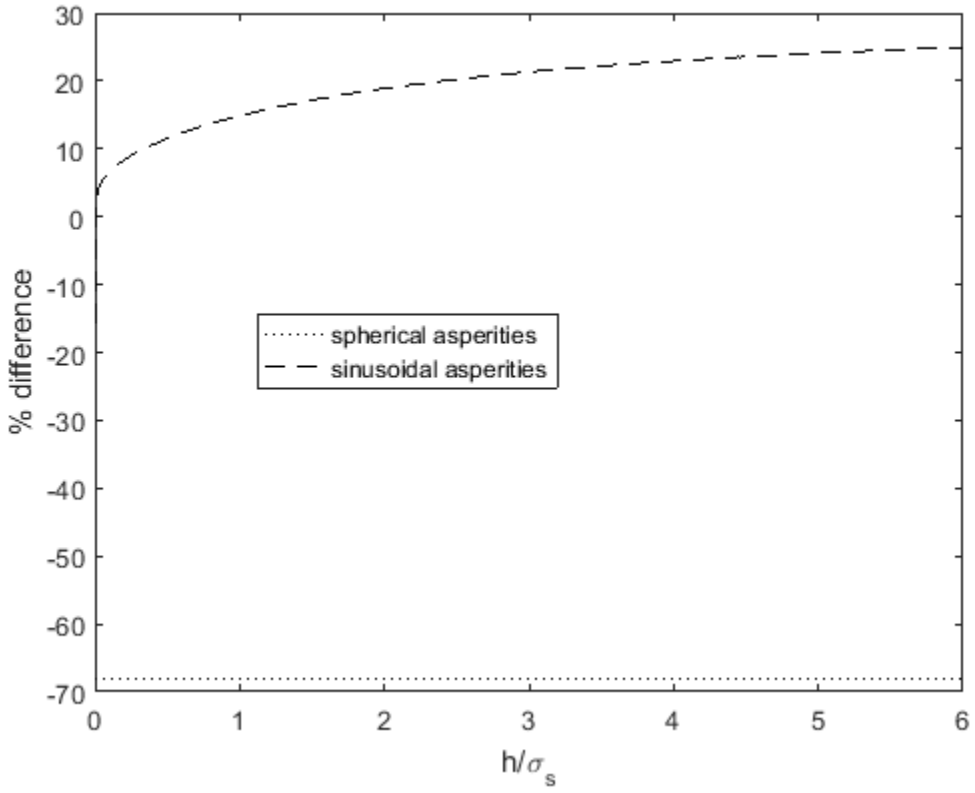

Figure 4.7: Percent difference, cylinder wall-rigid flat interface

Figure 4.7 shows the difference in contact area ratio for the sets of parameters when using them in the statistical model. The spherical asperity model predicts a difference of approximately 70%, which is more than double what the sinusoidal asperity model predicts. In Figure 4.8 and all subsequent figures that compare the statistical models, only the parameters generated from averaging two orthogonal directions are used because that would be more representative of the surface.

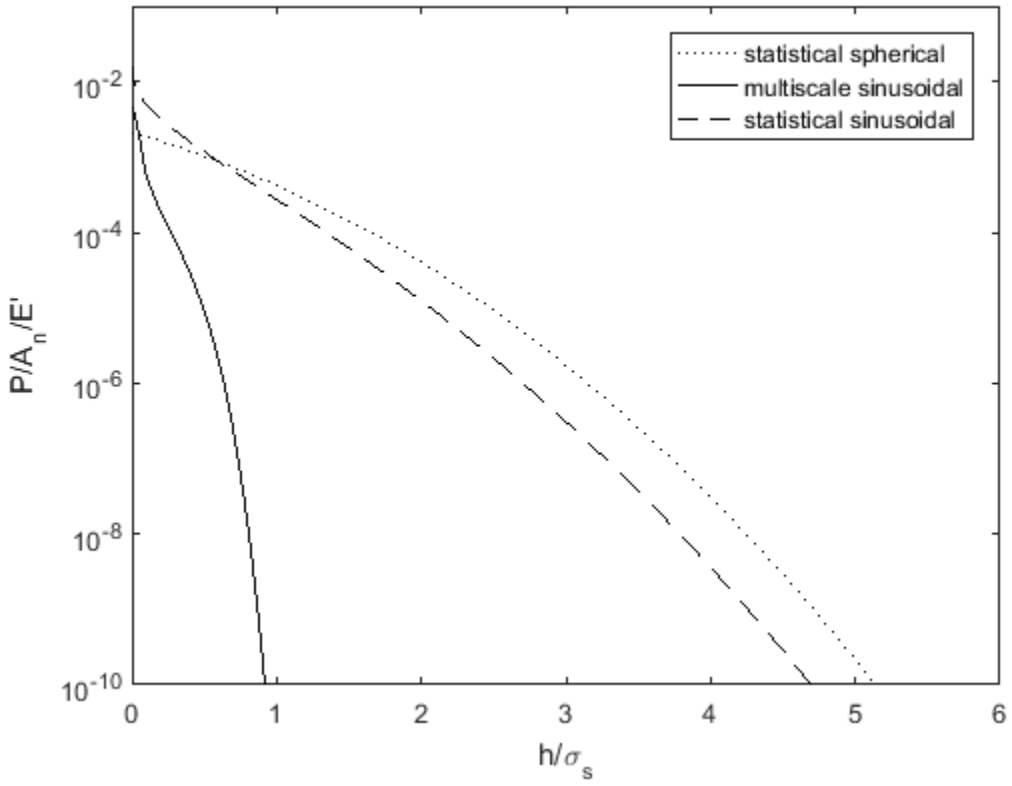

Figure 4.8: Contact pressure variation with surface separation, cylinder wall-rigid flat interface

Figure 4.8 compares the predicted contact pressure for the multiscale model and the statistical models for the cylinder wall. The statistical models predict a larger contact pressure than the multiscale model, where the trend is similar with completely different quantitative values. All models predict a large contact pressure that rapidly decreases as the surfaces are separated, but the multiscale model predicts the fastest decrease. The sinusoidal asperity model predicts the largest contact pressure at low separations, but decreases faster than the spherical model as the surfaces are pulled apart. It is important to know the contact pressure for a given surface separation because that is an input in the FEM model as shown in Figure 1.1.

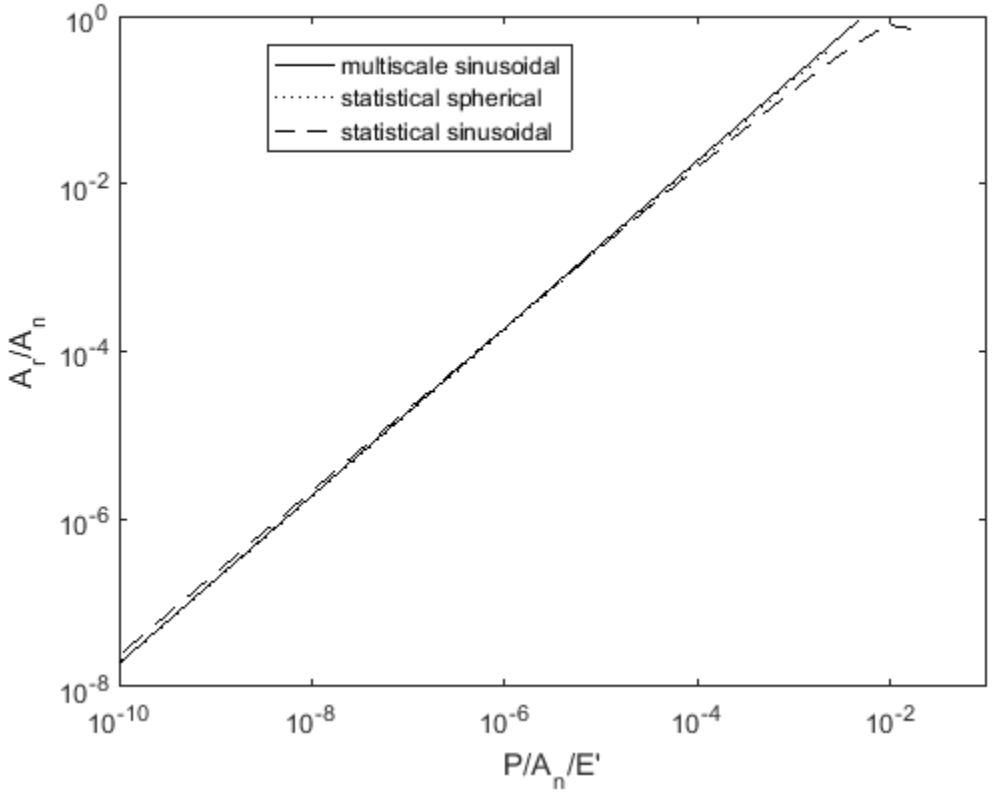

Figure 4.9: Area contact ratio for varied load, cylinder wall-rigid flat interface

Figure 4.9 compares the predicted contact area as a function of force for the three elastic-plastic models for the cylinder wall using parameters from Tables 4.1-4.3. All three of them display similar trends between contact area ratio and applied load. Upon closer inspection, the statistical sinusoidal model predicts the largest contact area at low loads and the smallest contact area at high loads. The relation also becomes nonlinear. This is likely because the asperities' deformations are no longer independent of each other, undermining one of the assumptions of the G-W model.

4.2 Cylinder Wall-Piston Ring Interface

The analysis setup was subsequently modified by replacing the rigid flat with a piston ring. The piston ring's surface heights were measured; Figure 4.10 shows a profile of its surface.

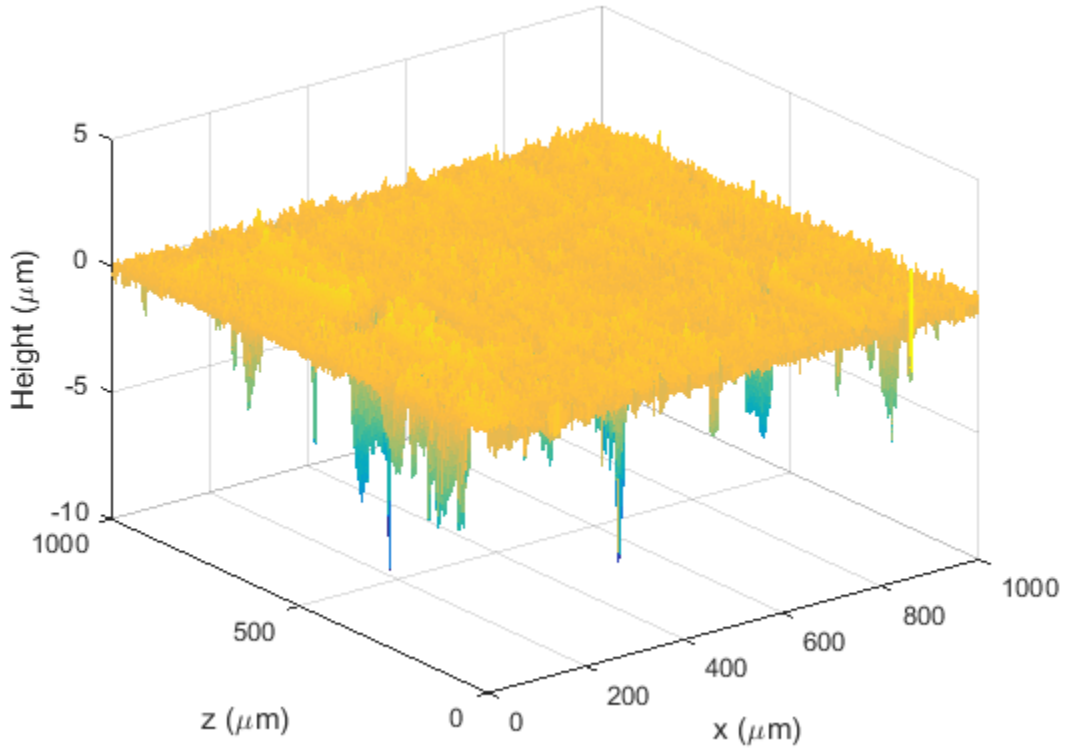

Figure 4.10: Surface profile of Piston Ring

The spectral moment approach was applied to both surfaces to generate three sets of statistical parameters, which are shown in Table 4.4. The analysis steps were identical for the combined surfaces, except that *E* was not set to infinity for the second surface. Instead, the ring's material properties were set to those in Table 4.2. To analyze the system using the multiscale model, the surfaces were transformed to the frequency domain, which resulted in the spectrum seen in Figure 4.11.

Table 4.4: Statistical parameters for both surfaces

	"x-direction"	"y-direction"	"averaged directions"
R (m)	$9.48*10^{-6}$	$1.26*10^{-5}$	$1.1*10^{-5}$
η ($1/m^2$)	$9.73*10^{9}$	$5.75*10^{9}$	$7.73*10^{9}$
σ_s (m)	$3.83*10^{-7}$	$3.46*10^{-7}$	$3.74*10^{-7}$

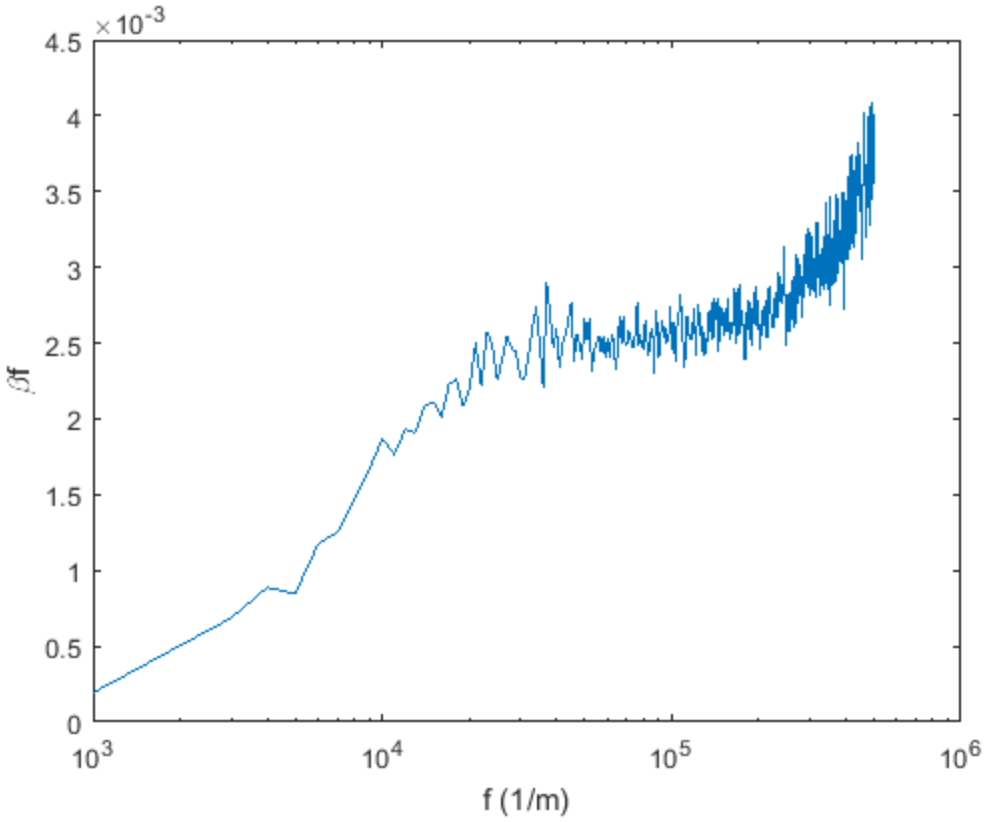

Figure 4.11: Spectrum of cylinder wall-piston ring interface

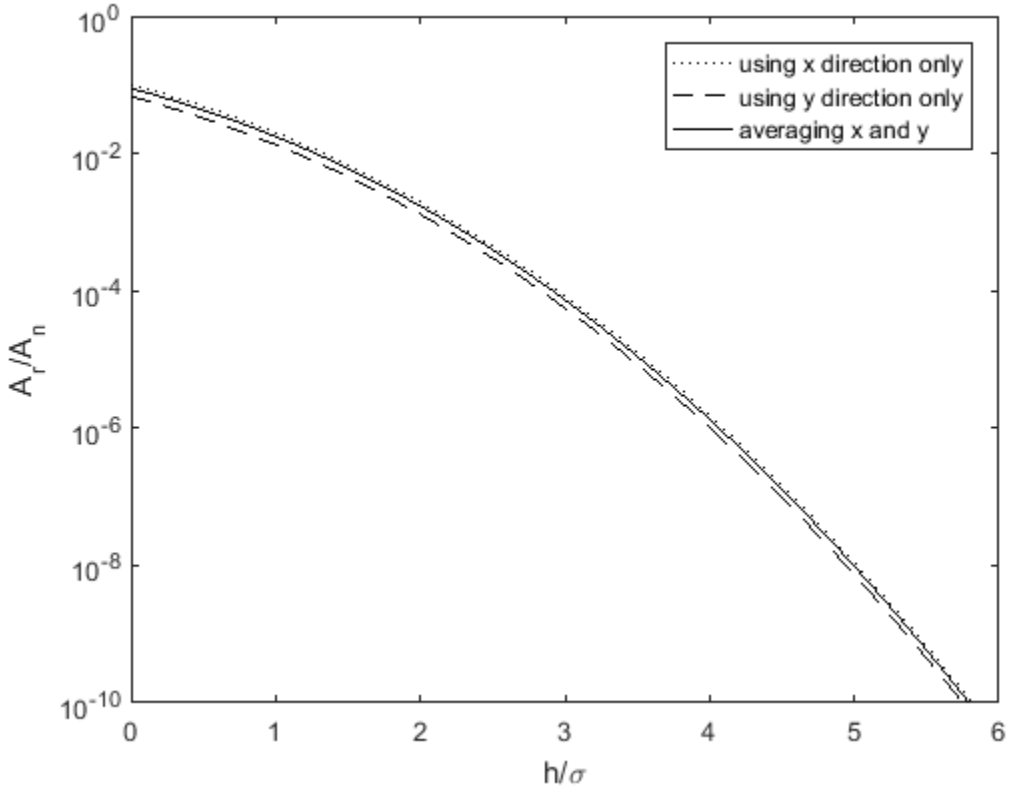

Figure 4.12: Area contact ratio over various surface separations predicted by elastic-plastic spherical statistical model, cylinder wall-piston ring interface

Figure 4.12 shows the trend of decreasing contact area as the surfaces are pulled apart. The area calculated by using properties computed from averaging directions lies between those values calculated using only one direction, which makes sense. The percentage of area in contact with the surface is only a small fraction, even at zero surface separation. This occurs because the valleys never come into contact, and the surface separation does not change due to deformation.

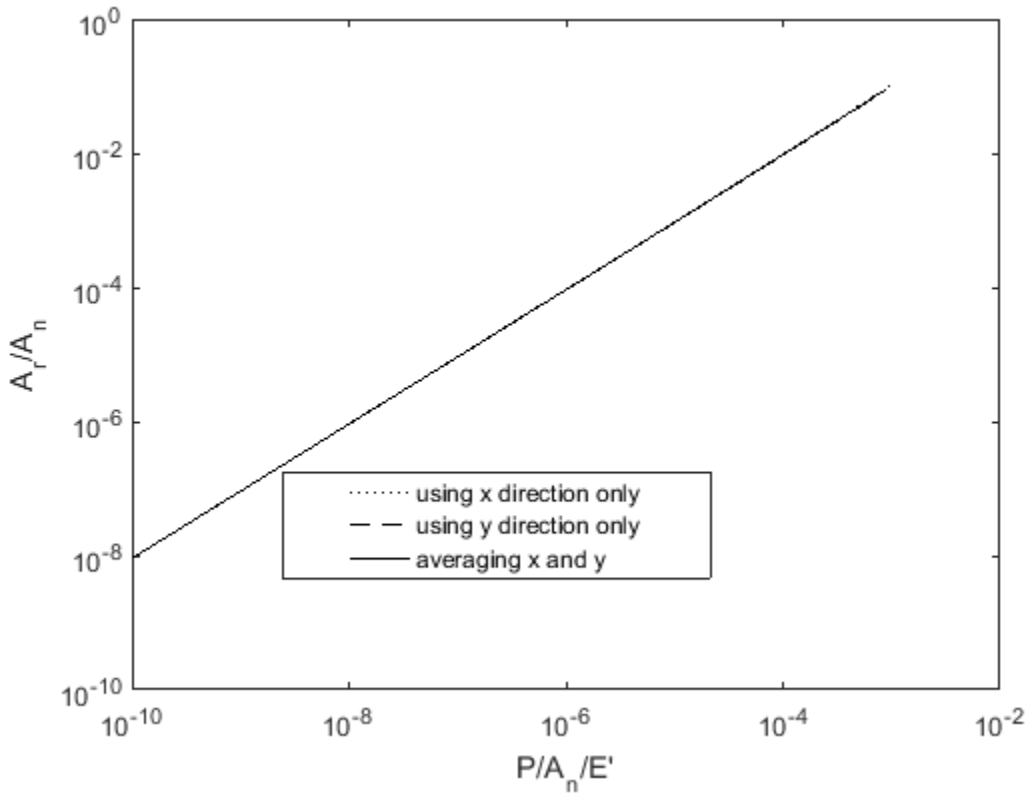

Figure 4.13: Variation of contact area with applied load predicted by elastic-plastic spherical statistical model, cylinder wall-piston ring interface

Figure 4.13 shows the variation of contact force and contact area. The effects of surface geometry are not significant to see a difference in predicted quantities.

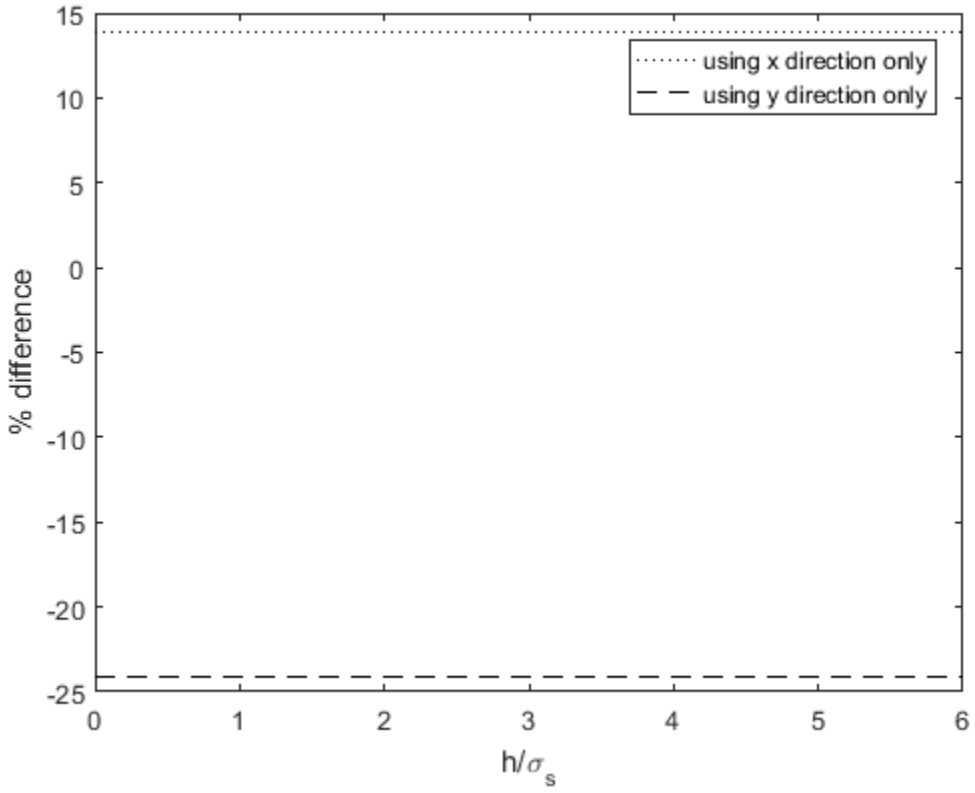

Figure 4.14: Difference from using different sets of parameters in the statistical model with spherical asperities, cylinder wall-piston ring interface

Figure 4.14 shows the relative difference caused by using statistical parameters calculated using only one direction instead of two. The percentage difference is lower compared to analyzing the wall relative to a rigid flat as seen in Figure 4.7.

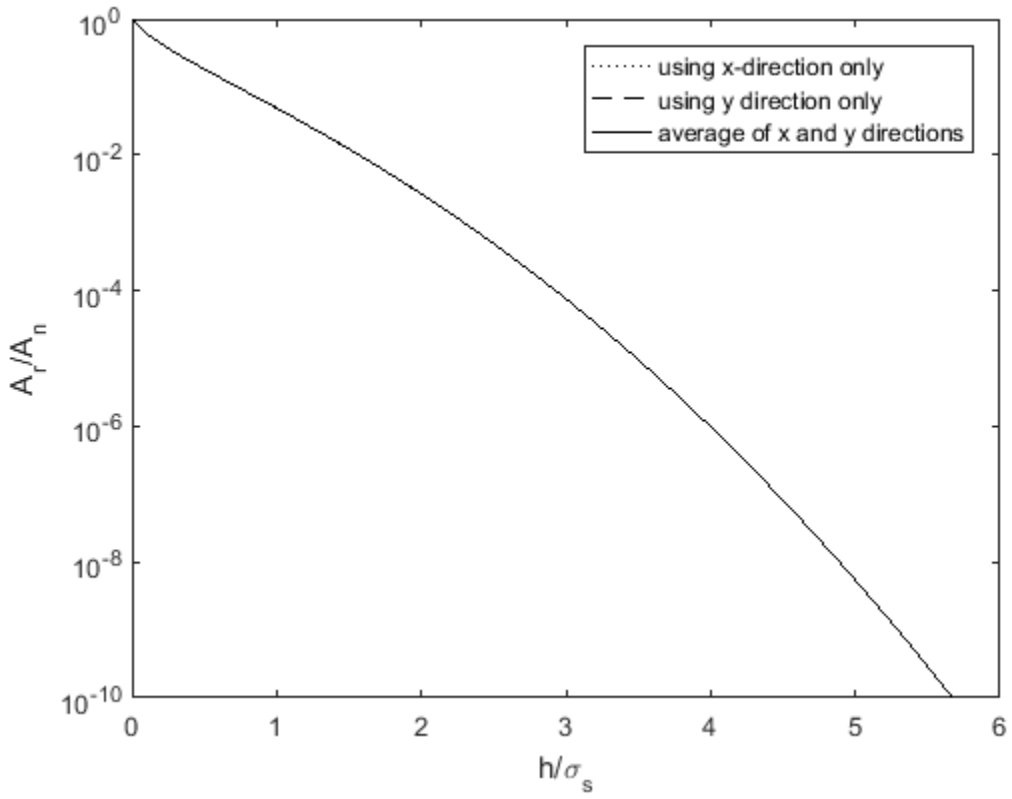

Figure 4.15: Area contact ratio with varied surface separation and sinusoidal asperities predicted by elastic-plastic spherical statistical model, cylinder wall-piston ring interface

Figure 4.15 displays the area contact ratio if sinusoidal asperities are combined with the statistical model to analyze the cylinder wall-piston ring interface using the statistical parameters in Table 4.4. The model exhibits similar trends compared to the analysis of the wall in contact with a rigid flat (see Figure 4.6). Furthermore, there is little difference in the direction-dependent results.

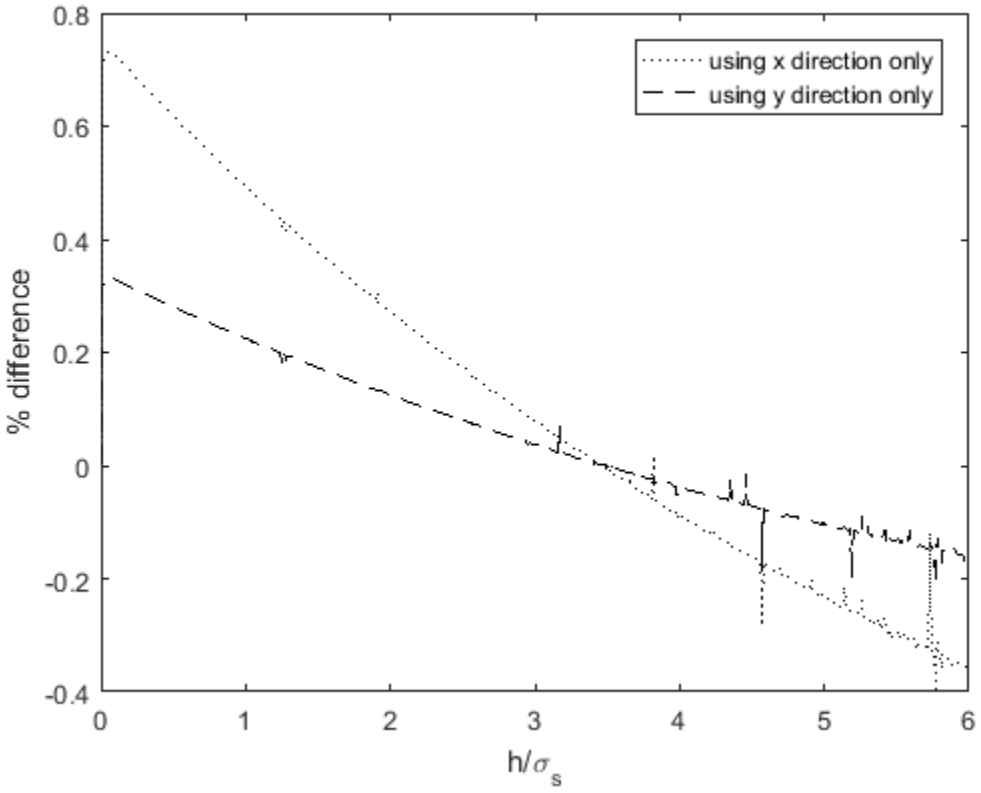

Figure 4.16: Difference from using different sets of parameters in the statistical model with sinusoidal asperities, cylinder wall-piston ring interface

Figure 4.16 shows the relative difference for the sinusoidal asperity model between the parameters from different directions. The differences are two orders of magnitude less for this model compared to the spherical asperity model. This is likely due to the periodic boundary condition imposed by the asperity model.

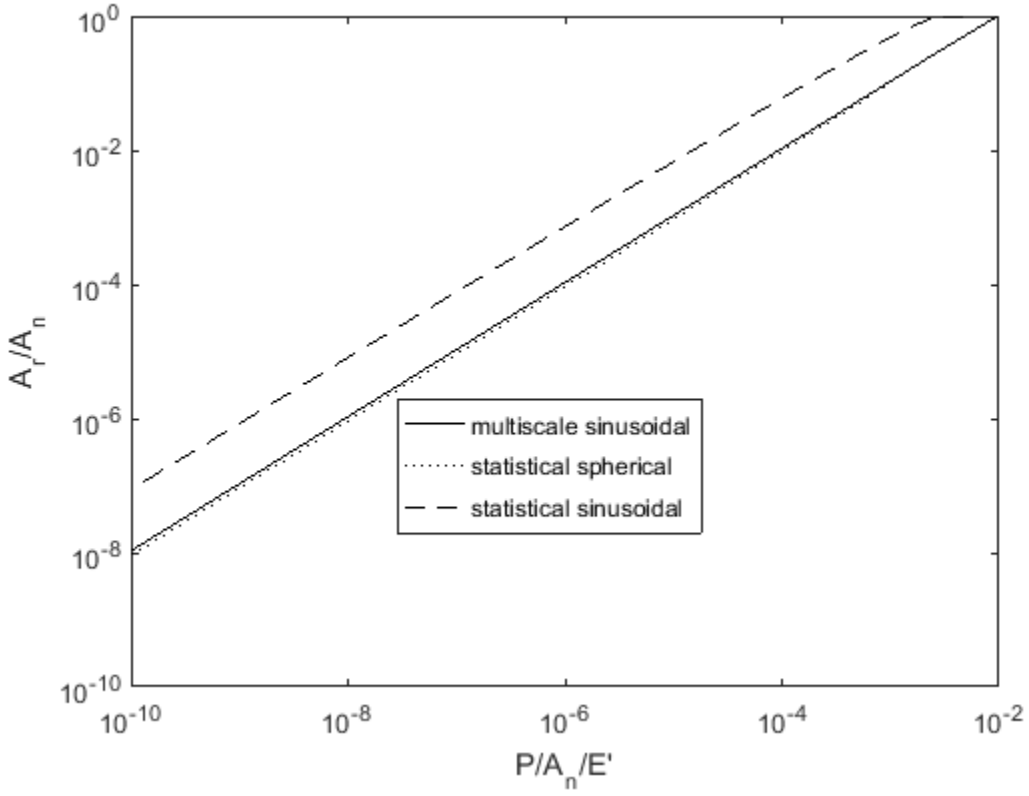

Figure 4.17: Area ratio for various applied loads, cylinder wall-piston ring interface

Figure 4.17 shows the relationship between the applied load and the contact area for all three contact models using the average surface parameters in Table 4.4 and the combined spectrum in Figure 4.11 for the multiscale model. The multiscale model and the statistical spherical model predict essentially identical contact areas for a given load, while the statistical sinusoidal model consistently predicts a larger area of contact for a given load. This is surprising because that model shares the same asperity model as the multiscale method.

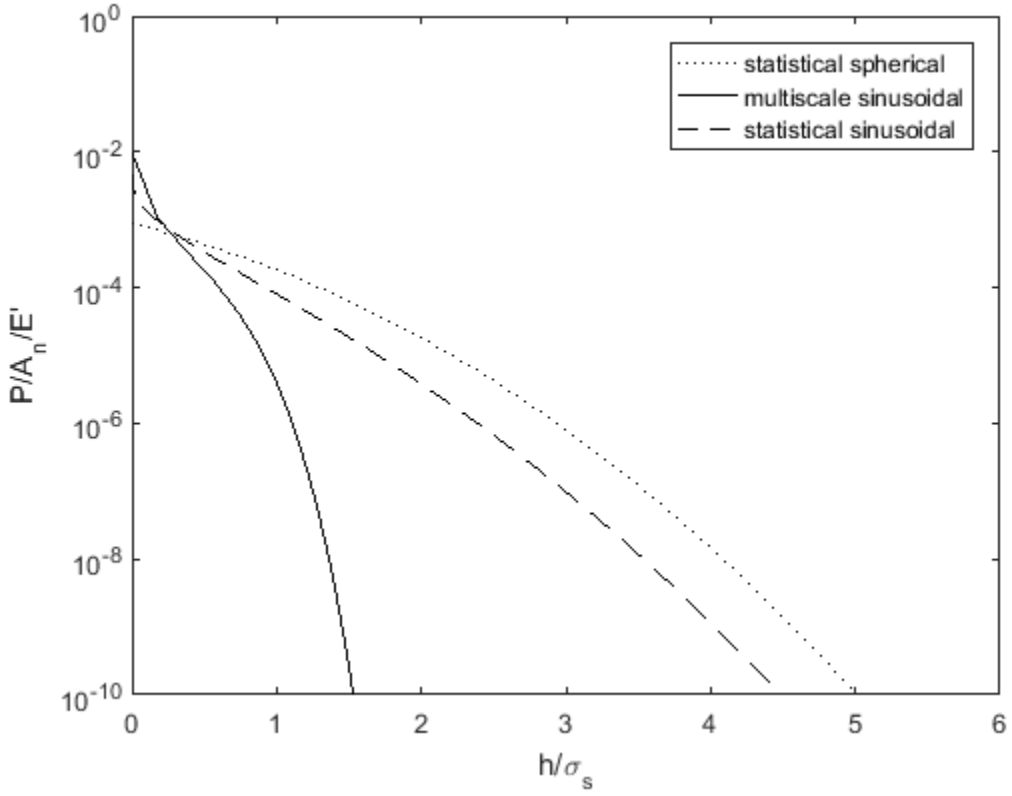

Figure 4.18: Pressure dependence on surface separation, cylinder wall-piston ring interface

Figure 4.18 depicts the variation of contact pressure with respect to surface separation. If sinusoidal asperities are used in the analysis, a greater contact pressure is predicted, but only for a small gap. The multiscale model is only useable for very low surface separations, as it otherwise predicts a pressure several orders of magnitude lower than the statistical models. This may be because the model does not consider the asperity distribution or inter-scale asperity contact. Likewise, the spherical asperity model predicts a larger contact pressure for larger surface separations. The curves resemble those found by Wilson et. al. [19] when they compared statistical and multiscale models.

CHAPTER 5

COMPARING THE STATISTICAL AND MULTISCALE MODELS WITH DETERMINISTIC RESULTS

5.1 Surface Characterization

To verify the models, they were compared to two surfaces analyzed by Wang [20]. His study included varied resolutions on both surfaces. Both surfaces were 32x32 μm with four resolutions: 1 μm, 0.5 μm, 0.25 μm, and 0.125 μm. The smallest resolution was obtained using a profilometer, while spectral interpolation was used to create intermediate values of height between data points. The two surfaces were leveled and zeroed using the same procedures mentioned in Chapter 4. Equations 3.9-3.13 were applied to all of them, and relevant results are summarized in Table 5.1. Both sets of parameters are for the 33x33 surfaces.

Table 5.1: Statistical Parameters for the reference surfaces

Surface	4L		63M	
	"y direction"	"averaged directions"	"y direction"	"averaged directions"
R (m)	$2.64*10^{-6}$	$4.19*10^{-6}$	$1.64*10^{-6}$	$2.13*10^{-6}$
η ($1/m^2$)	$1.11*10^{11}$	$5.86*10^{10}$	$6.37*10^{10}$	$3.64*10^{10}$
σ_s (m)	$3.55*10^{-7}$	$3.52*10^{-7}$	$5.73*10^{-7}$	$5.48*10^{-7}$

In all other cases, α was found to be less than the required value to assume a Gaussian distribution. Those sets of parameters were discarded.

The valid parameters were converted to a frequency and wavelength corresponding to sinusoidal asperities. They were combined with material properties in

Table 5.2 and used in the G-W model. Also, the surfaces were converted to the frequency domain to analyze them using the multiscale model. Figures 5.1 and 5.2 show the spectral plots for the surfaces in Table 5.1.

Table 5.2: Material properties for the reference surfaces

Property	Value
E	200 GPa
v	0.3
S_y	1 GPa

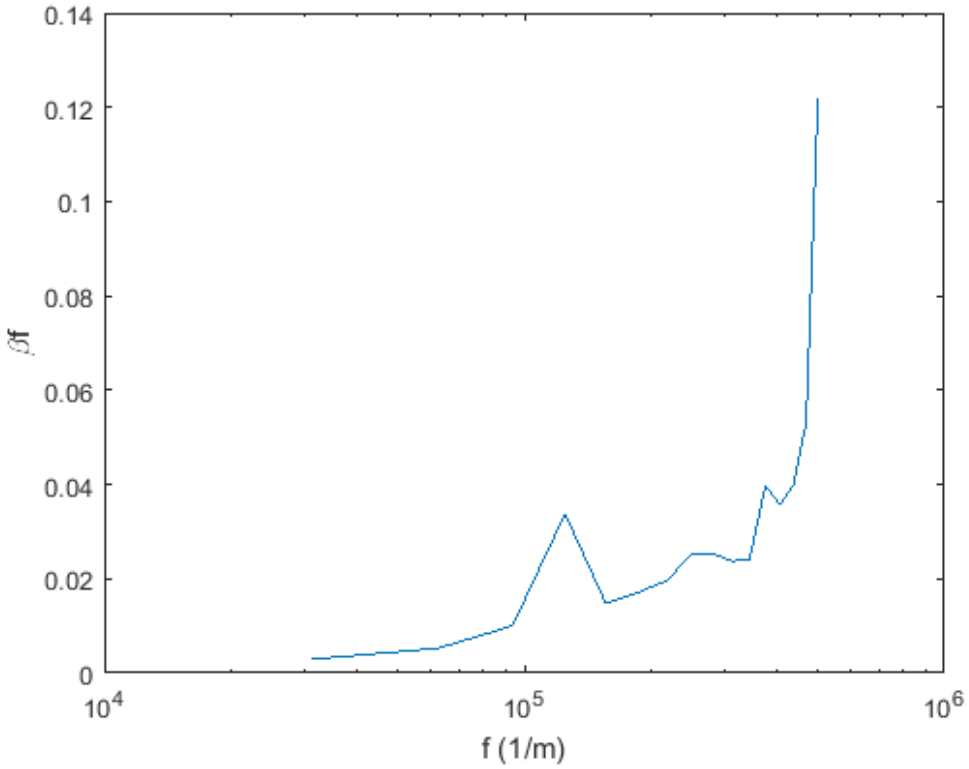

Figure 5.1: Spectrum of Surface 4L

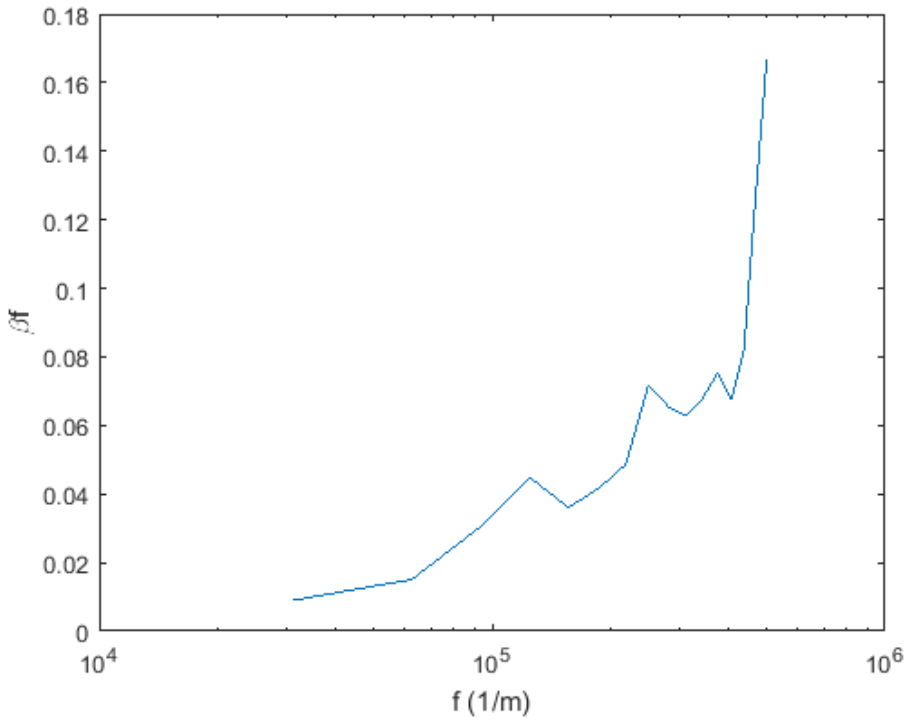

Figure 5.2: Spectrum of Surface 63M

5.2 Surface 4L Analysis

The same steps detailed in Chapter 4 for the statistical models were repeated using the parameters in Tables 5.1 and 5.2. Also, the surfaces were transformed to the frequency domain to analyze them using the multiscale model. The detailed process was presented in Chapter 3.

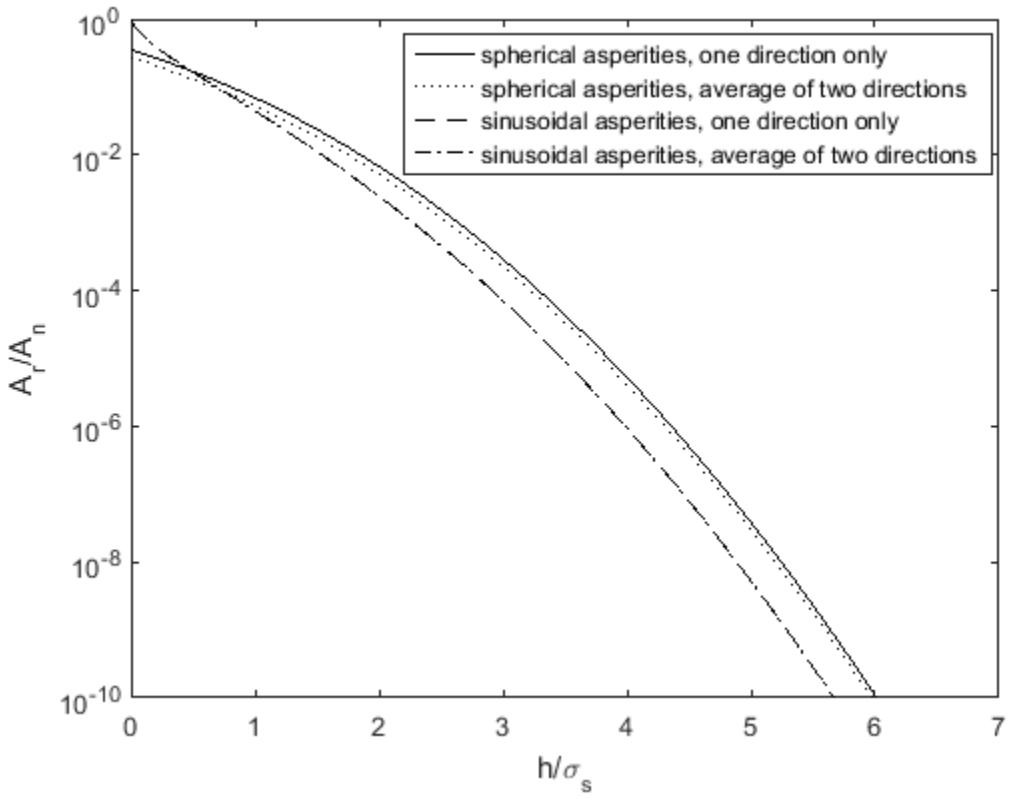

Figure 5.3: Contact area ratio for Surface 4L using statistical models

Figure 5.3 depicts contact area for various surface separations when the statistical models were applied to Surface 4L. The sinusoidal asperity model again predicts a higher contact area at very small surface separations relative to the spherical asperity model.

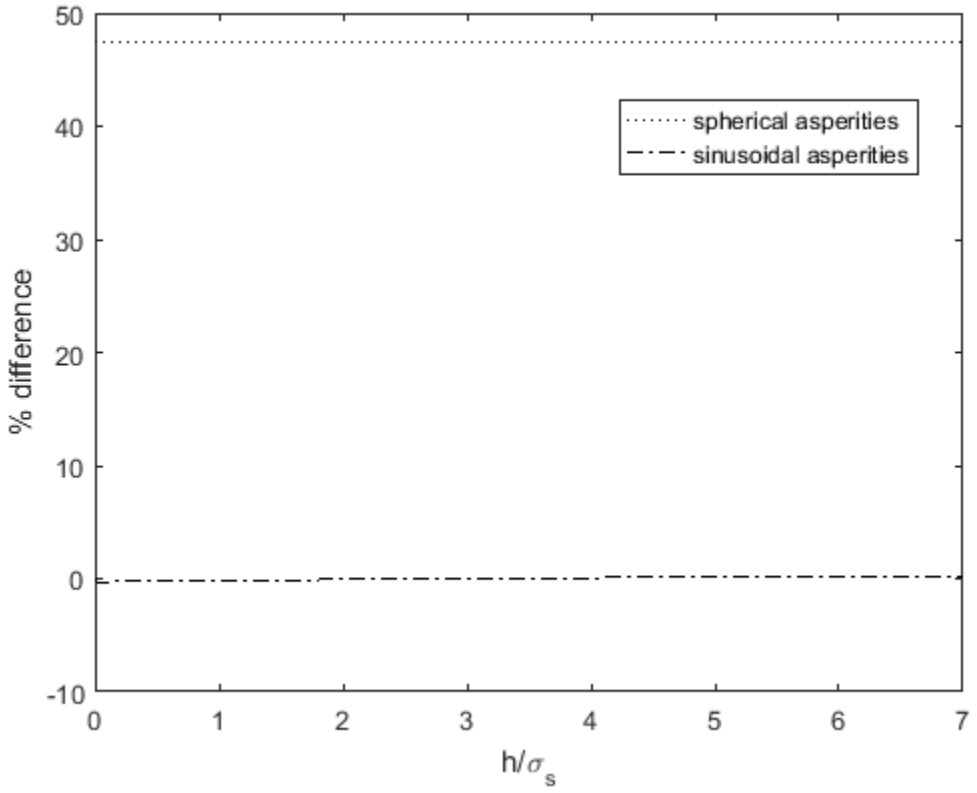

Figure 5.4: Difference caused by using different sets of parameters for surface 4L

The effect of using different sets of parameters can be seen for both models in Figure 5.4. The spherical model consistently predicts approximately 30% more contact area for a given surface separation if analyzed using only one direction of spectral moments. The sinusoidal model does not exhibit that trait, except at very large surface separations where contact pressure is negligible.

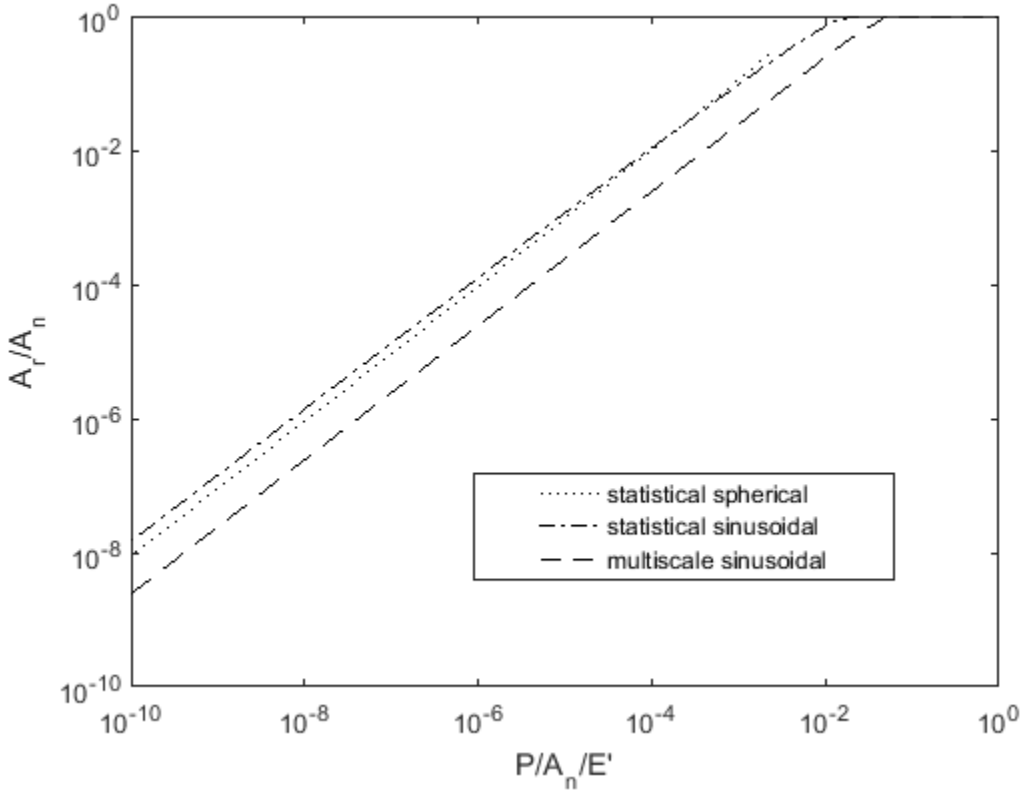

Figure 5.5: Comparison of applied load and contact area ratio for surface 4L

Figure 5.5 compares the trend between contact pressure and area of contact for all three models. They predict a linear relationship, but the multiscale model predicts a significantly smaller contact area relative to the statistical models. The spherical model predicts a smaller contact area for smaller loads, but a larger contact area for larger loads relative to the sinusoidal model. In any plot that compares statistical and non-statistical models, only the average of directions is shown for the statistical models because that would provide a more valid comparison between the surfaces.

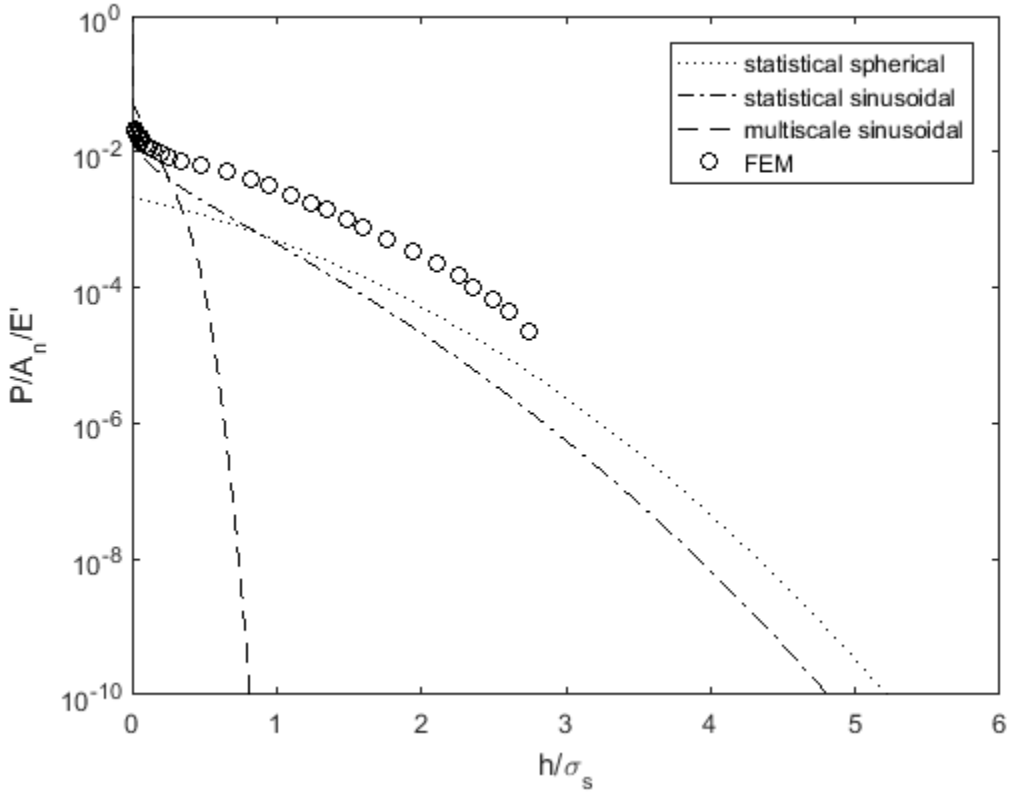

Figure 5.6: Contact pressure for surface 4L

Figure 5.6 compares contact pressure for a wide range of surface separations and contact models. The multiscale model once again predicts a much different trend for load-dependent surface separation. At very low surface separations, it predicts a much higher contact pressure relative to the statistical models. However, the contact pressure falls off much more rapidly as the surface separation increases. Wang [20] predicts a similar trend to the statistical models, but the load is an order of magnitude larger for a given surface separation. The statistical models do not consider changes in the surface distribution or the mean surface height during deformation, which could explain the discrepancies.

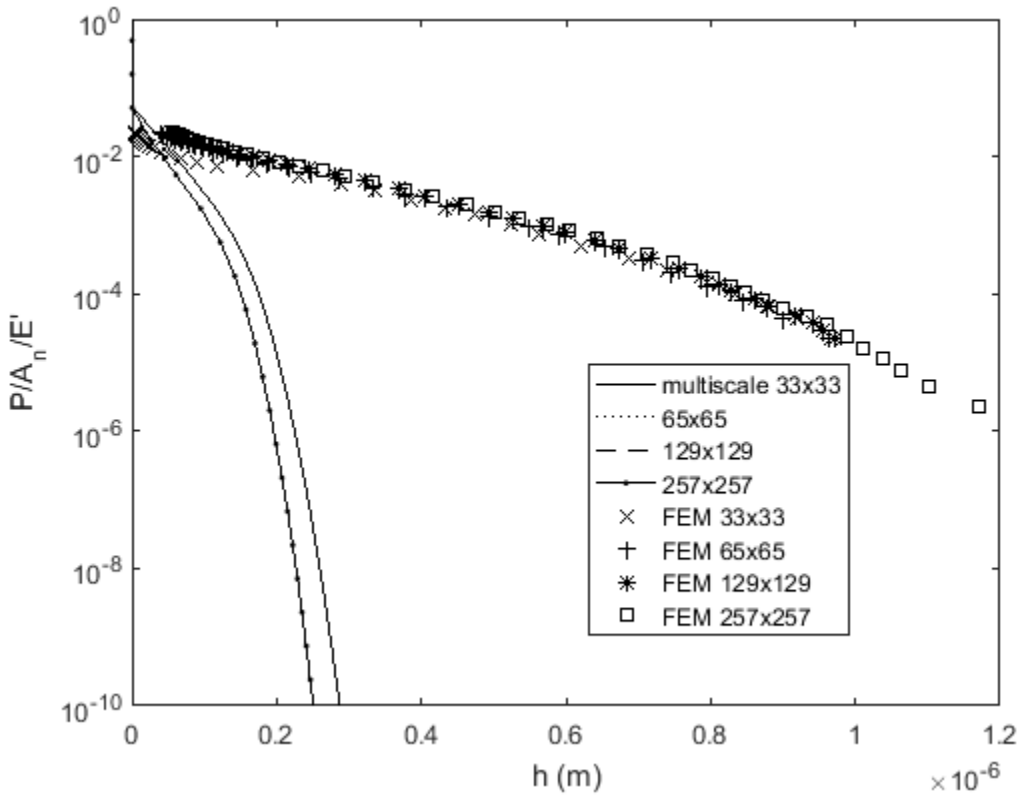

Figure 5.7: Contact pressure for varied sample spacing, surface 4L

Figure 5.7 shows the results of the multiscale model applied to all provided resolutions and compared with results from Wang [20]. Statistical models were not analyzed for the larger resolutions because a real value of σ_s could not be calculated. None of the multiscale models agree with Wang's results; they predict a larger contact pressure when the surface separation is less than 50 nm. Otherwise, they predict a much smaller contact pressure. The FEM results do not change much for different resolutions, which confirms that method's accuracy.

5.3 Surface 63M Analysis

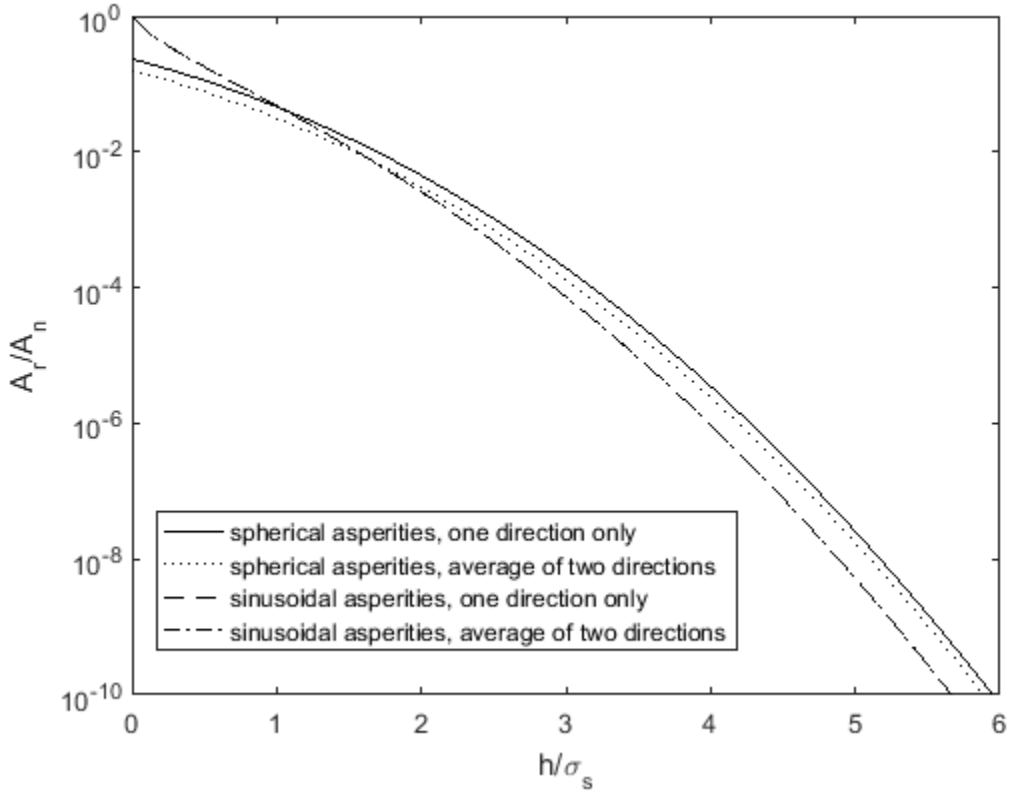

Figure 5.8: Area contact ratio for surface 63M

Figure 5.8 displays the contact area for various surface separations; the trends match those found for other surfaces. The contact area ratio decreases as the surfaces become farther apart, and the sinusoidal asperity model predicts a larger decrease. The effects of surface anisotropy are apparent for the spherical model, but not the sinusoidal model.

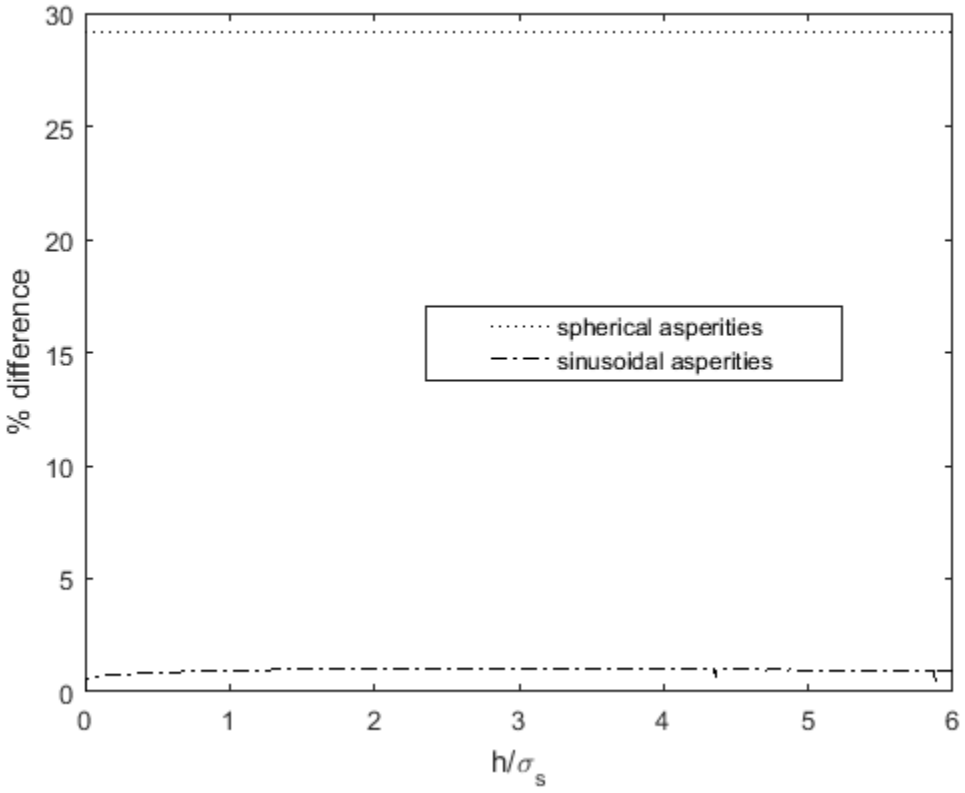

Figure 5.9: Differences caused by using different sets of parameters in statistical models for surface 63M

Figure 5.9 illustrates the difference caused by using different sets of parameters in the statistical models. The difference for using only one set of spectral moments with spherical asperities is near 30%, which is quite large.

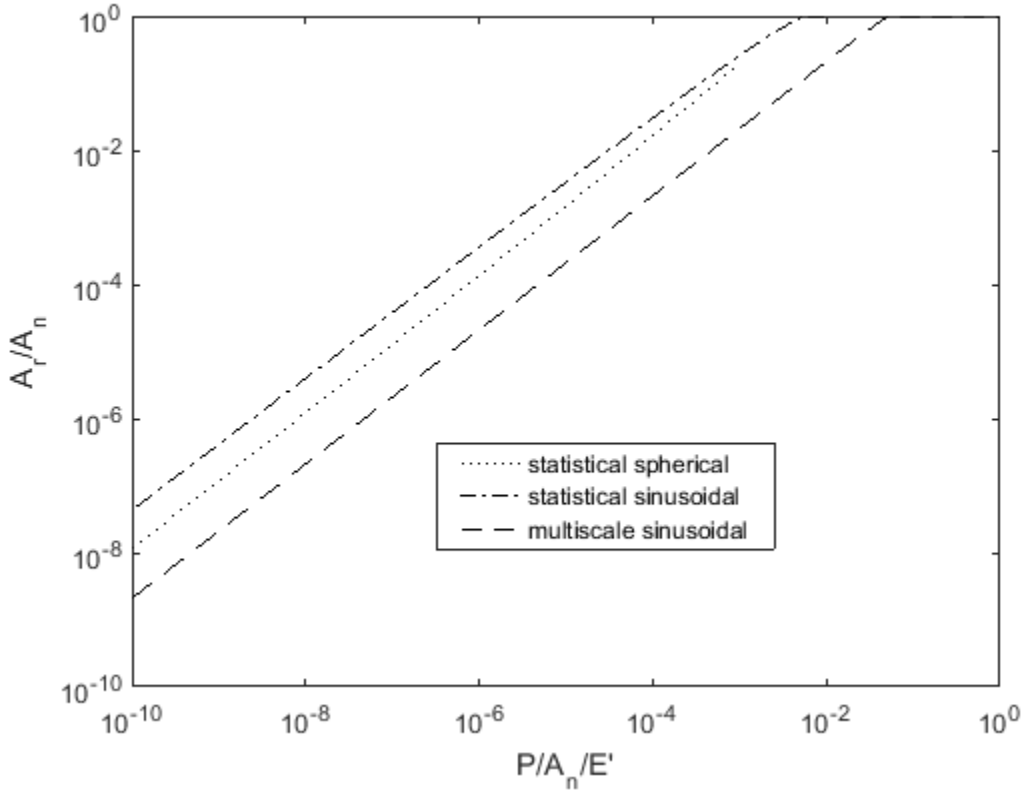

Figure 5.10: Comparison of applied load and contact area ratio for surface 63M

Figure 5.10 shows the relationship between contact area and applied force for all three models applied to surface 63M. The multiscale model once again predicts a much smaller area of contact for a given force relative to the statistical models. If sinusoidal asperities are used in the statistical model, the predicted contact area is larger than if spherical asperities are used.

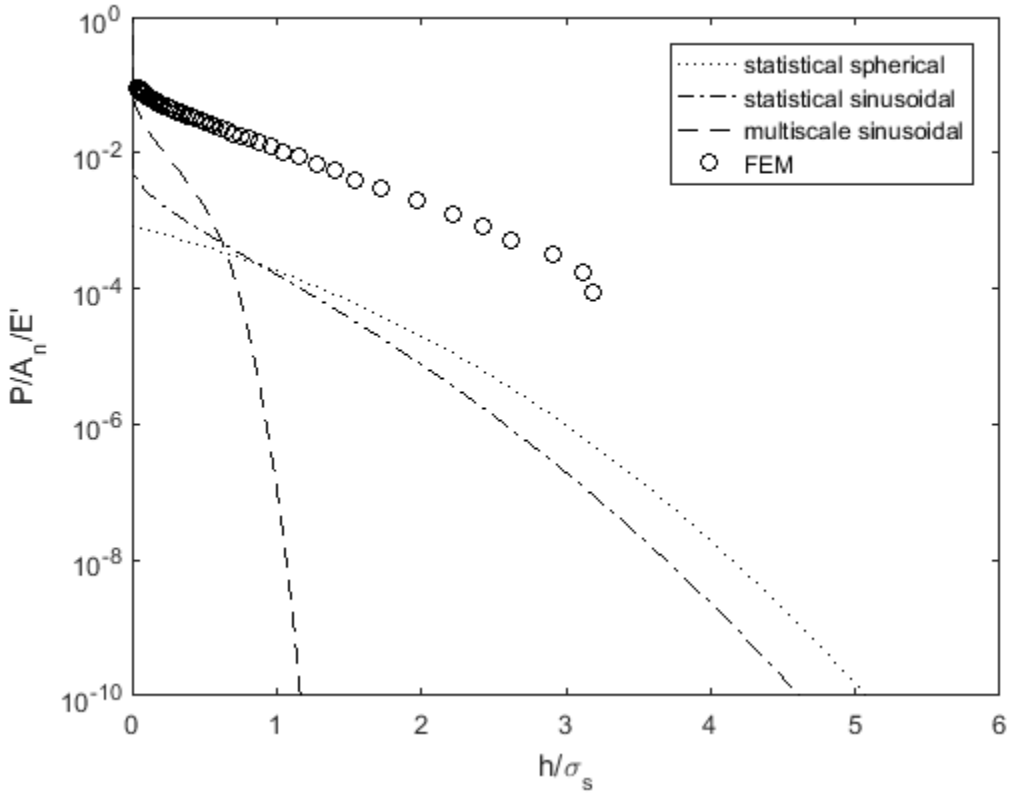

Figure 5.11: Contact pressure on surface 63M

Figure 5.11 shows contact pressure on surface 63M for varying surface separation. All three models predict a lower pressure than Wang. The statistical models exhibit a similar behavior to his results with a proportional offset. The multiscale model predicts a similar pressure at zero surface separation, but much lower pressures if the separation is increased.

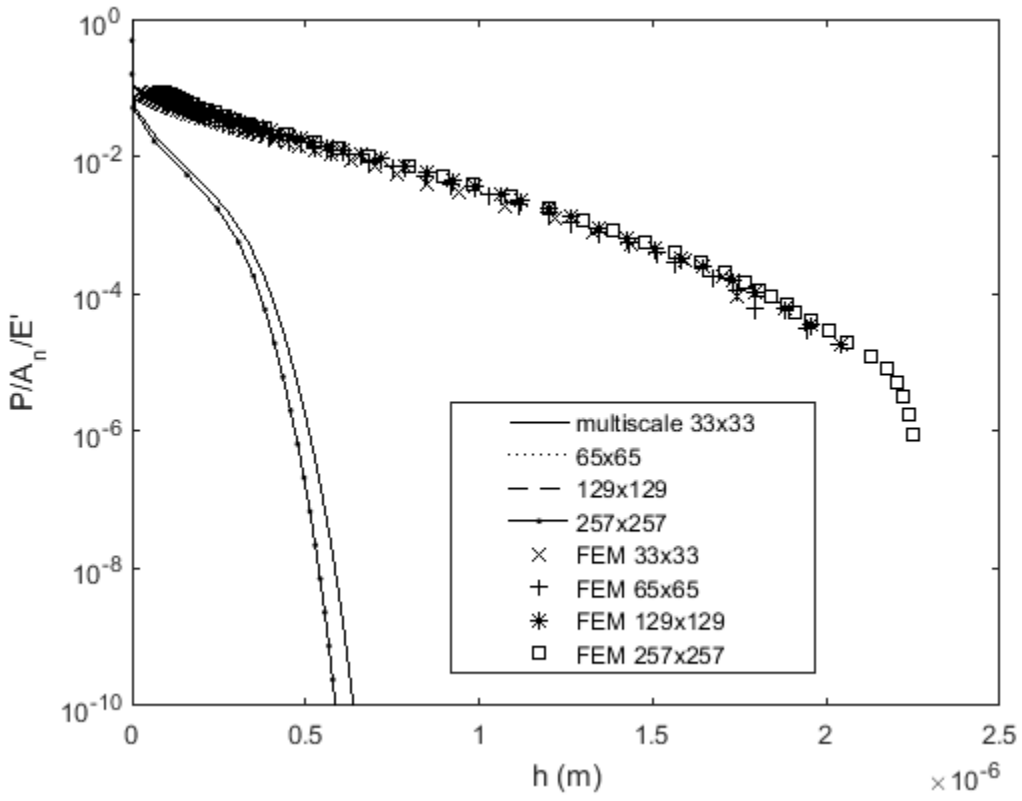

Figure 5.12: Contact pressure for surface 63M with varied surface spacing

Figure 5.12 compares the contact pressure calculated by the multiscale model for various surface resolutions to deterministic results. Statistical models could not be used because a real value of σ_s was not calculated. For zero surface separation, the multiscale model and the deterministic model predict similar values.

CHAPTER 6

CONCLUSIONS AND FUTURE WORK

Three different rough surface contact models were explored in this work to analyze a piston ring-cylinder wall interface. Two of them were statistical; the only difference between them was how they treated individual asperities. Both are vulnerable to errors when applied to an anisotropic surface. Moreover, they depend on the surface heights being close to a Gaussian distribution. If spherical asperities are used, the predicted contact area for a given surface separation is lower than if sinusoidal asperities are used. However, the predicted contact pressure is higher except at very low surface separations.

The third model analyzed was the full multiscale model. Unlike statistical models, the distribution of surface heights is irrelevant. However, the predicted contact pressure exhibits a much different trend relative to the statistical models and differs quantitatively except for very small separations. This happens because the model does not consider the asperity distribution or inter-scale asperity contact. Otherwise, it predicts a similar trend between contact area and applied load. The relative contact area for a given force compared to the other models depends on the surface, though.

To validate the models, they were tested against a deterministic model calculated using finite elements on reference surfaces. The results exhibited similar trends to the results using the wall and ring. The multiscale model predicted the lowest contact area for a given load, while the statistical sinusoidal model predicted the largest. The

statistical models predicted a similar trend but different values for contact pressure given surface separation. The statistical models are believed to underestimate the contact pressure because they do not vary the mean height or the surface distribution as surface separation decreases. Ultimately, the individual surface must be characterized first; generalizations cannot be made.

The work shown in this thesis is only one part of a larger project involving a coupled rough surface contact-lubrication model in an internal combustion engine to predict friction and wear. These contact pressures will be combined with fluid pressures calculated using the Reynolds equation, and an iterative model will be constructed along the flow chart of Figure 1.1. The effects of heat generation and various coatings on the surfaces will be analyzed in the future. In the 3D finite element model, the possibility of material failure will be considered.

REFERENCES

[1] Greenwood, J.A. and J.B.P. Williamson, *Contact of Nominally Flat Surfaces*. Prol. R. Soc. Lond. A, 1966(295): p. 300-319.

[2] Chang, W.R., I. Etsion, and D.B. Bogy, *An Elastic-Plastic Model for the Contact of Rough Surfaces*. ASME J. Tribol., 1987. 109(2): p. 257-263.

[3] Jackson, R. L. and I. Green, *A Statistical model of Elastic-Plastic Asperity Contact between Rough Surfaces*. Trib. Int., 2006. 39(9): p. 906-914.

[4] Kogut, L. and I. Etsion, *A Finite Element Based Elastic-Plastic Model for the Contact of Rough Surfaces*. Tribology Transaction, 2003. 46(3): p. 383-390.

[5] Majumdar, A. and B. Bhushan, *Fractal Model of Elastic-plastic Contact Between Rough Surfaces*. ASME J. of Tribol., 1991, 113(1): p. 1-11.

[6] Jackson, R.L. and J.L. Streator, *A multi-scale model for contact between rough surfaces*. Wear, 2006. 261(11-12): p. 1337-1347.

[7] Johnson, K.L., *Contact Mechanics*. 1985, Cambridge, U.K.: Cambridge University Press. 452.

[8] Ciavarella, M., G. Demelio, et al., *Linear Elastic Contact of the Weierstrass Profile*. Proc. R. Soc. Lond. A., 2000(456): 387-405.

[9] Johnson, K.L., J.A. Greenwood, and J.G. Higginson, *The Contact of Elastic Regular Wavy Surfaces*. Int. J. Mech. Sci., 1985. 27(6): p. 383-396.

[10] Archard, J.F., *Elastic Deformation and the Laws of Friction*. Proc. R. Soc.Lond. A., 1957(243): p. 190-205.

[11] Krithivasan, V. and R.L. Jackson, *An Analysis of Three-Dimensional Elasto-Plastic Sinusoidal Contact*. Tribology Letters, 2007. 27(1): p. 31-43.

[12] Gao, Y.F., A.F. Bower, *Elastic-Plastic Contact of a Rough Surface with Weierstrass Profile*, Proc. R. Soc. A. 2006(462), p. 319-348.

[13] McCool, J.I., *Comparison of Models for the Contact of Rough Surfaces*. Wear, 1986 (107): p. 37-60.

[14] Jackson, R. L., S. Saha, and Y. Xu, The Influence of Single Asperity Models on Predicting Contact Between Elastic Rough Surfaces Using Statistical Methods, *STLE Tribology Frontiers Conference*, Denver, CO, Oct. 25-27, 2015.

[15] Jackson, R.L., V. Krithivasan, and W. E. Wilson, *The Pressure to Cause Complete Contact Between Elastic-Plastic Sinusoidal Surfaces*. IMechE J. of Eng. Trib. – Part J. 222(1): 857-863.

[16] Ghaednia, H., X. Wang, S. Saha, Y. Xu, A. Sharma, R.L. Jackson, *A Review of Elastic-Plastic Contact Mechanics*. Appl. Mech., 2017. 69(6), 060804.

[17] Rostami, A., R.L. Jackson, *Predictions of the average surface separation and stiffness between contacting elastic and elastic-plastic sinusoidal surfaces*. J. of Eng. Trib. (2013). 227(12): p. 1376-1385.

[18] Green, C.K., J.L. Streator, C. Haynes, E.Lara-Curzio, *A Computational Leakage Model for the Solid Oxide Fuel Cell Compressive Seals*. J. Fuel Cell Sci. Tech., 2011 8(4).

[19] Wilson, W.E., S.V. Angadi, R.L. Jackson, Surface Separation and contact resistance considering sinusoidal elastic-plastic multi-scale rough surface contact. Wear, 2010. 268:190-201.

[20] Wang, X., *Static Friction and Junction Growth of Contacting Three-Dimensional Sinusoidal Asperities and Rough Surfaces*. Auburn University, 2017.